3 Results

3.1 Purification and spectroscopic properties of PrP27-30 samples purified from Syrian hamsters

The amount of protein found in the purified PrP27-30 samples was in the range 7.5-30 µg/BE without a strict relation to the particular TSE strain (see Appendix 1).

3.1.1 Silver staining

Protein samples, obtained from scrapie 263K infected or healthy hamster brains (Figure 3.1 A and B) and purified according to the "original" procedure developed by Prof. Diringer and co-workers, showed a high degree of purity of the investigated PrP27-30. The staining properties of the material were comparable with those described elsewhere (Diringer *et al.*, 1997). Samples from infected brains showed a major stained band at 27-30 kDa and a shadow at 25 kDa and intense bands at about 20 kDa (Figure 3.1 A). Under the same conditions, samples equivalent to 0.1 or 0.2 BE of the residual protein faction obtained from uninfected brains (Figure 3.1 B) showed minor staining at about 33 kDa, which corresponds to the molecular weight of the PK (Figure 3.1 C) and a characteristic double band at about 20 kDa, assigned to ferritin (Diringer *et al.*, 1997).

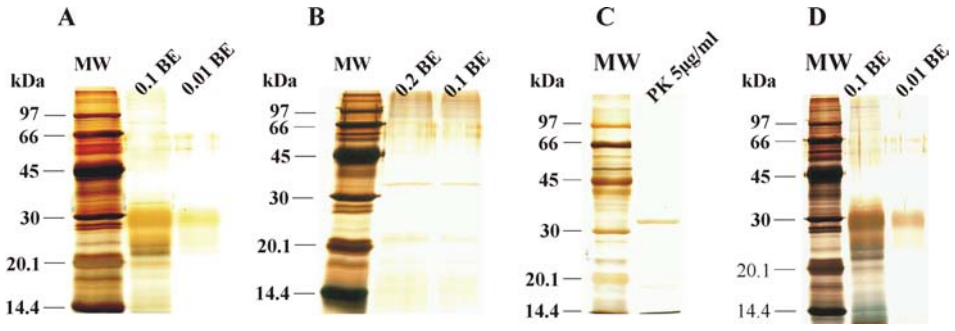

Figure 3.1 Characteristic silver stained SDS-PAGE gels of purified protein samples: A, scrapie-infected hamster brains according to the "original" extraction and purification procedure (Diringer *et al.*, 1997); B, healthy hamster brains and scrapie-infected hamster brains according to the modified procedure; C, silver stained proteinase K sample; D, scrapie-infected hamster brains according to the modified extraction and purification procedure (see section 2.2). MW-molecular weight markers.

The silver staining of PrP27-30 fractions obtained after purification according to the modified extraction and purification procedure (Figure 3.1 D) showed no essential differences in the composition and the staining of the samples.

Silver staining of PrP27-30 samples purified from hamster brains infected with different TSEs showed comparable degree of purity as shown in Figure 3.2.

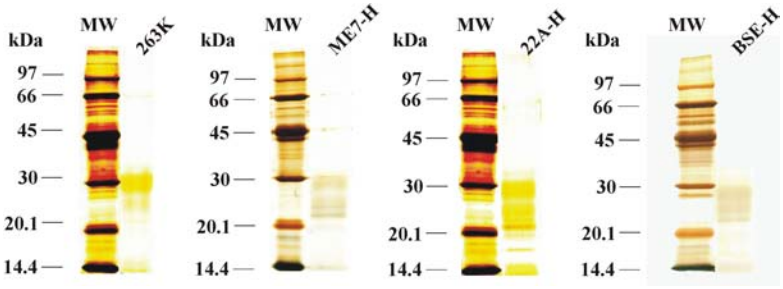

Figure 3.2 Silver staining of SDS-PAGE gels of PrP27-30 samples purified from 263K, ME-7-H, 22A-H and BSE-H. Each sample represents 0.01 BE

However, silver stained PAGEs of purified PrP27-30 fractions obtained in independent procedures revealed minor variations in the staining properties in respect to sample impurities and the relative intensity of the stained protein bands as indicated by arrows in Figure 3.3.

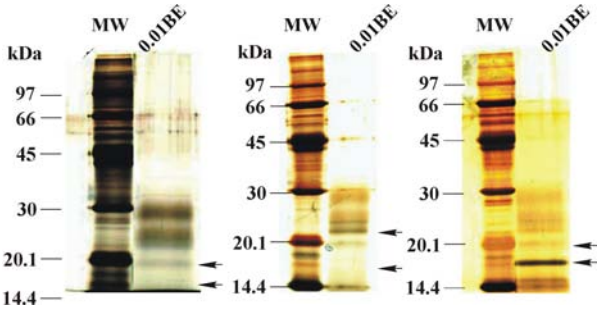

Figure 3.3 Variations in the silver staining properties of PrP27-30 samples purified in independent preparation runs.

Band variations at about 20 kDa possibly reflect variations in the ferritin content. However, some amyloid preparations from the four TSE isolates are characterized by the presence of an intensively stained band at ~17-18 kDa, of yet unknown origin.

3.1.2 Immunostaining

The immunostaining with 3F4 mAb showed a clear and characteristic triplet staining pattern of PrP27-30 and a positive signal in samples representing 10^{-5} BE (see Figure 3.4).

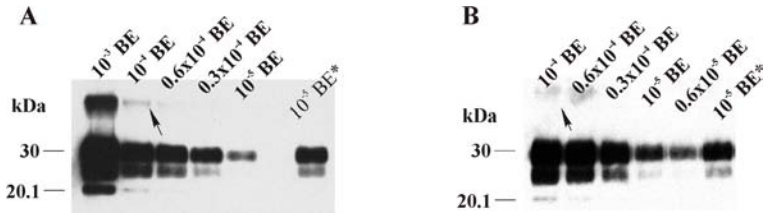

Figure 3.4 Immunostaining with 3F4 mAb of PrP27-30 from 263K purified according to the original (A) and the modified (B), purification procedures. *-positive control (see section 2.3.2.2).

In samples representing 10^{-3} and 10^{-4} BE, a band at about 64 kDa was observed that corresponded to PrP27-30 dimers (indicated by arrows).

3.1.3 FT-IR spectra

The second derivative FT-IR spectra of PrP27-30 purified from 263K scrapie, according to the "original" procedure showed pronounced absorption features in both, the amide I and II absorption regions (

Figure 3.5).

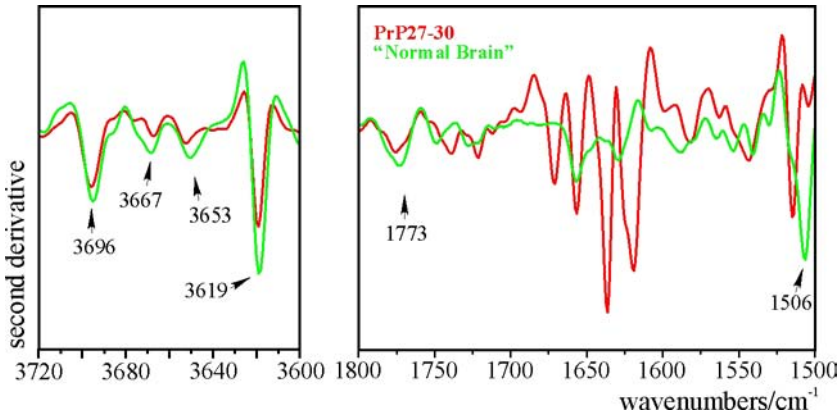

Figure 3.5 FT-IR spectra of PrP27-30 (red curve) (10 µg/µl) and the residual proteins, extracted and purified from healthy hamster brains (green curve) (3 µg/µl). The latter represent the maximum protein amount found in 1 BE (see Appendix 1). The arrows show untypical for proteins absorption band components found in spectra from scrapie infected or healthy hamster brains.

In addition, the spectra revealed the presence of characteristic absorption pattern in the region between 3720 and 3600 cm^{-1} and two individual band components at 1506 and 1773 cm^{-1} (indicated by arrows,

Figure 3.5), which are untypical for proteins. These bands varied in intensity between spectra from independent PrP27-30 preparations. They were also found in samples from normal hamster brains, suggesting that these band components have a cellular origin or are associated with the chemical compounds used in the purification procedure. The second derivative spectra obtained from normal brain material were characterized by two main amide I absorption bands located at 1629 and 1657 cm^{-1}.

3.1.4 FT-IR characteristics of chemical compounds used in the PrP27-30 extraction and purification procedure

In order to determine the origin of these undefined spectral features, all chemical compounds used in the extraction and purification procedures were examined for IR absorptions throughout the whole mide-infrared region. This spectral screening reveal, that EDTA and the detergent sarcosyl show pronounced absorption features in the amide I and amide II regions associated with C=O stretching and COO^- bending absorptions, respectively. However the spectral characteristic in the frequency range 1300-1800 cm^{-1} (see the blue and green reference lines, Figure 3.6) show that both chemical components are not present in the absorption spectra of the PrP27-30 aggregates.

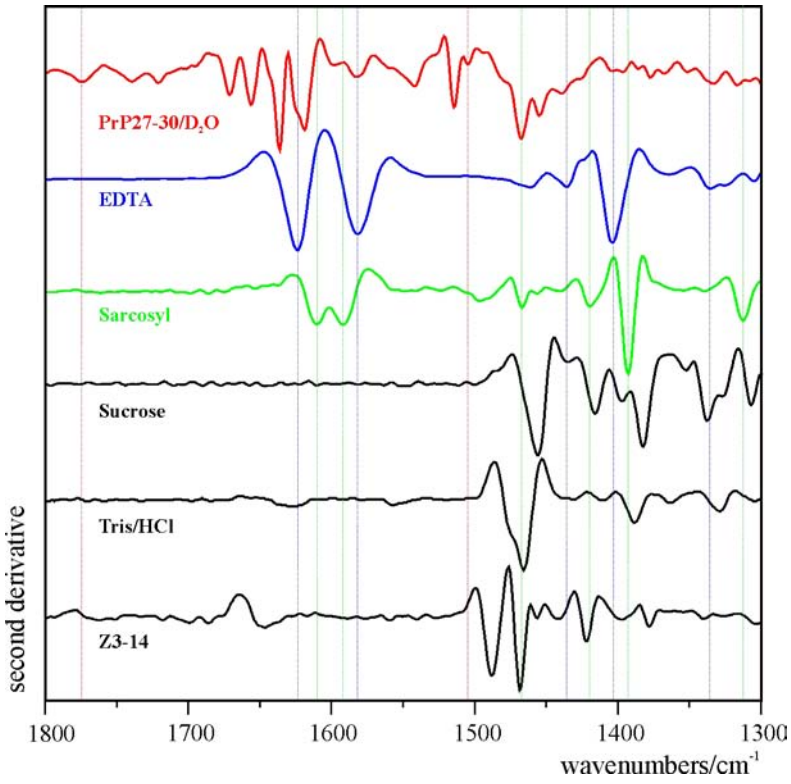

Figure 3.6 FT-IR absorption characteristics of the chemical compounds used in the PrP27-30 extraction and purification procedure.

Furthermore, none of the chemical compounds, shows absorption band components that could be associated with the IR features, untypical for proteins, observed in the PrP27-30 absorption spectra (see the red lines, Figure 3.6). The only possible "external" source of contamination could be polycarbonate particles, occasionally disintegrated from the walls of the tubes during the high speed centrifugations or the ultrasound applied to resuspend the protein pellets (see section 2.2.). Polycarbonate consists of repeated units (see Figure 3.7) with aromatic and carbonyl functional groups that could produce the spectral features observed.

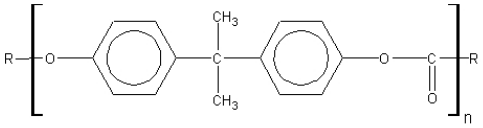

Figure 3.7 Chemical structure of the polycarbonate monomer.

Indeed, a small dark-gray pellet was obtained when polycarbonate tubes filled with ddH_2O were vigorously sonicated and consequently centrifuged at 145 000g (45 000 rpm) for 60 min in a 60 Ti-rotor. The FT-IR spectra of these particles produced a spectral pattern matching the spectral features found in the examined protein samples (Figure 3.8).

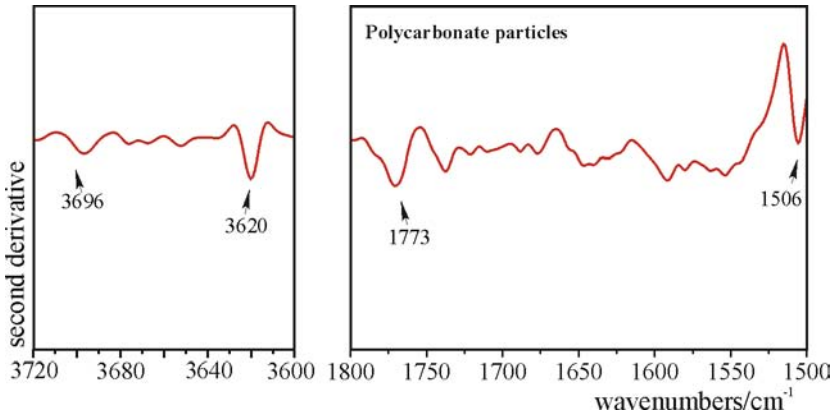

Figure 3.8 FT-IR spectroscopic characteristics of polycarbonate particles disintegrated from the centrifuging vials

Therefore, in order to avoid contamination with polycarbonate particles in all consequent PrP27-30 preparations, ultrasound was applied only in glass instead of polycarbonate tubes. In addition a new polycarbonate vial was used at each step of the purification procedure involving centrifugation (see section 2.2).

The FT-IR spectra of PrP27-30 samples from 263K purified according to the modified procedure resulted in purified material practically free of disintegrated polycarbonate particles (Figure 3.9).

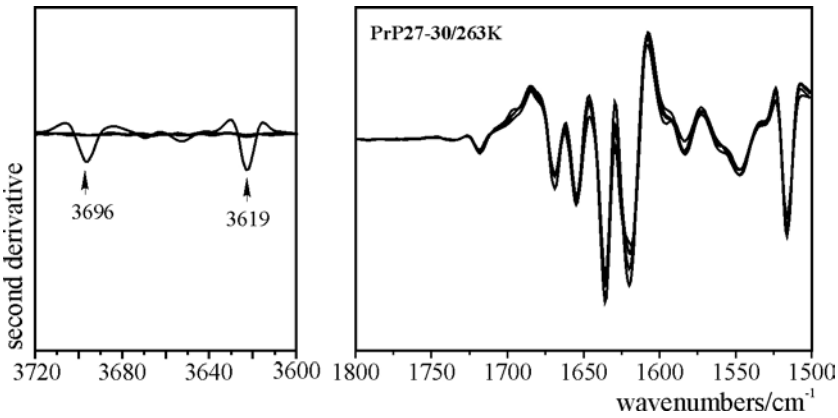

Figure 3.9 FT-IR spectra of PrP27-30 purified from 263K according to the modified extraction and purification procedure. Spectra from independent purification runs were normalized between 1600-1750 wavenumbers.

Minor absorption bands in the range 3720-3600 wavenumbers were seen only in some of the subsequent preparations (indicated by arrows) but none of the samples showed "contaminant" IR absorption in the amide I or II regions.

3.1.5 Effects of protein concentration on the PrP27-30 spectral characteristics

Despite, the use of the detergent Z3,14, the suspensions of PrP27-30 aggregates remained very rough, that made difficult to prepare samples with exact, relatively high concentration in small volumes. The variations in concentration of the 263K PrP27-30 samples are reflected in the amide I component band at 1620 cm^{-1} (Figure 3.10).

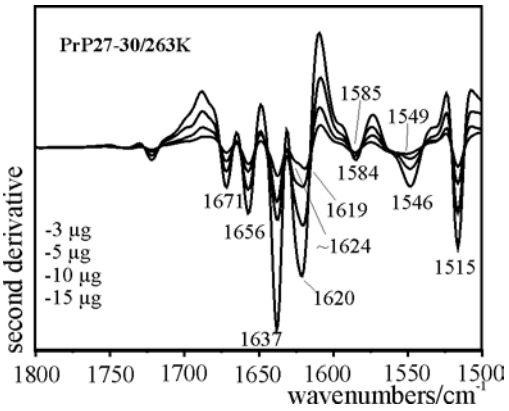

Figure 3.10 Effect of the variation in the PrP27-30 concentration on the FT-IR spectral pattern

In samples with high protein concentration the exact peak position was at 1620 cm^{-1}. With the decrease of protein concentration a shoulder appeared at about 1624 cm^{-1} and the main component shifted from 1620 cm^{-1} to 1619 cm^{-1}. The amide II band component showed a decrease in intensity and a shift of the main peak from 1547 to 1549 cm^{-1} with the decrease of the PrP27-30 concentration. These effects are possibly due to higher H/D exchange in the less concentrated samples. This suggests, that the characteristic changes of the spectral component at 1620 cm^{-1} can also be related to variations of the H/D exchange rate in the samples.

3.1.6 Reproducibility of the FT-IR measurements.

FT-IR spectra obtained from D_2O suspensions of PrP27-30 samples purified in independent preparation runs showed high reproducibility of the results (see Figure 3.9). The result showed that the minor variations in the sample purity do not disturb the PrP27-30 specific second derivative spectral pattern. Indeed, second derivative FT-IR spectra of prion rods collected before and after treatment with PK (Figure 3.11) reveal that the characteristic secondary structure band components of PrP27-30 predominates even in samples containing significant amounts of “contaminant” proteins (see insert in Figure 3.11).

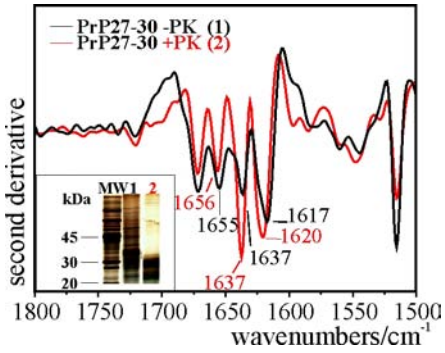

Figure 3.11 Secondary structure characteristics of PrP27-30 samples derived before (black spectrum) and after (red spectrum) treatment with PK. The spectra were normalized between 1600 and1750 cm^{-1}. The silver stained samples represent the amount of protein corresponding to 0.2 BE. MW-molecular marker; PrP27-30 before (1) and after treatment with PK (2).

3.2 Strain differences

FT-IR spectroscopy could shed light on the main question of this project: whether the secondary structure characteristics of the PrP27-30 aggregates differ sufficiently to make possible the strain discrimination of different TSEs?

3.2.1 FT-IR spectral characteristics of PrP27-30 aggregates from hamster adapted TSEs

The FT-IR absorption spectra of all pathological prion protein PrP27-30 samples investigated here were characterized by broad and complex amide I and II contours between 1500 and 1700 cm^{-1}, which exhibited strain specific features as will be shown later. Figure 3.12 shows typical absorption spectra of PrP27-30 purified from ME7-H scrapie-infected brains obtained from dried samples (A), and samples hydrated in H_2O (B) or D_2O (C). As seen from the FT-IR absorption spectra, the scrapie agent is characterized by prominent amide I and II bands.

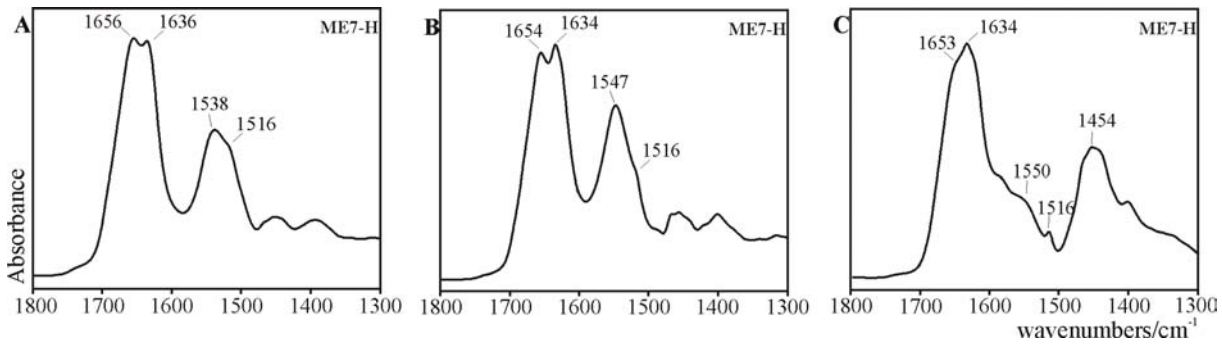

Figure 3.12 Typical absorption spectra obtained from strain ME7-H PrP27-30 A) dried samples B) H_2O suspensions and C) D_2O suspensions. The spectra were normalized between 1600- 1750 cm^{-1}. The frequency values of some characteristic and pronounced spectral features are given.

The amide I mode originates mainly from the >C=O stretching vibration of the polypeptide backbone (Bandekar 1992; Fabian *et al.,* 2000; Barth *et al.,* 2002). The major factors responsible for the conformational specificity of the amide I band are its sensitivity to hydrogen bonding and the characteristic coupling between transition dipoles, the latter leading to characteristic splitting effects. The magnitude of this splitting depends on the orientation and distance of interacting dipoles and thus provides information about the geometrical arrangements of peptide groups in a polypeptide chain (Krimm *et al.,* 1972; Surewicz *et al.,* 1993). In all absorption spectra of PrP27-30 at least two amide I absorption maxima can be located between 1630 and 1660 cm^{-1} (see Appendix 2) which indicates different secondary

structure elements in PrP27-30 of ME7-H (Bandekar 1992; Fabian *et al.*, 2000; Barth *et al.*, 2002).

The amide II band between 1600 and 1500 cm^{-1} essentially originates from the amide N-H bending vibration coupled to N-H stretching with some contributions from >C=O bending and C-C plus C-N stretching vibrations (Bandekar 1992; Fabian *et al.*, 2000). The amide II absorption maximum of the dried PrP27-30 samples was found between 1534 and 1540 wavenumbers, while in the spectra of H_2O-hydrated samples it was centred at 1547 cm^{-1} in the spectra of samples hydrated in H_2O. This band most probably arises from the absorption of an α-helix (Sokolowski *et al.*, 2003). In protein spectra obtained from D_2O (Figure 3.12 C), the substitution of H by D atoms resulted in a shift of the amide II absorption band with about 100 wavenumbers to around 1454 cm^{-1} (amide II´). In this frequency range the N-D absorption of proteins is merged together with the absorption of symmetric and asymmetric deformations of the CH_2 and CH_3 functional groups in the amino acid side chains, lipids and carbohydrates (see Table 1.IV). The remaining absorption in the amide II region shows that not all amide groups are available for H/D exchange. Regardless of the sampling technique, all spectra exhibit a constant feature at 1516 cm^{-1}, which is assigned to a tyrosine vibration (Barth 2000).

3.2.2 Band assignment from the second derivative analysis of PrP27-30 from hamster adapted TSEs

A problem in the IR analysis of proteins is that the experimentally observed bands are complex composites of overlapping components representing different secondary structure elements. Thus here the second derivatives were used to enhance the apparent resolution for structural analysis of PrP27-30 from different hamster-adapted TSE agents. Although the secondary structure analysis of proteins by FT-IR spectroscopy is an established technique (Susi *et al.*, 1983; Dong *et al.*, 1990; Fabian *et al.*, 2002), the assignment of a given band component to a particular type of secondary structure is not a trivial task (Surewicz *et al.*, 1993). In the case of PrP27-30, the structural interpretation of the FT-IR spectra is additionally complicated by the highly aggregated state of the prion protein and the fact, that additional chemical constituents are constantly found in prion rods. Thus, our secondary structure assignments are still preliminary to some degree.

Figure 3.13 shows the overlaid second derivative spectra obtained from independent PrP27-30 preparations, of dried samples, and samples suspended in H_2O or D_2O. These

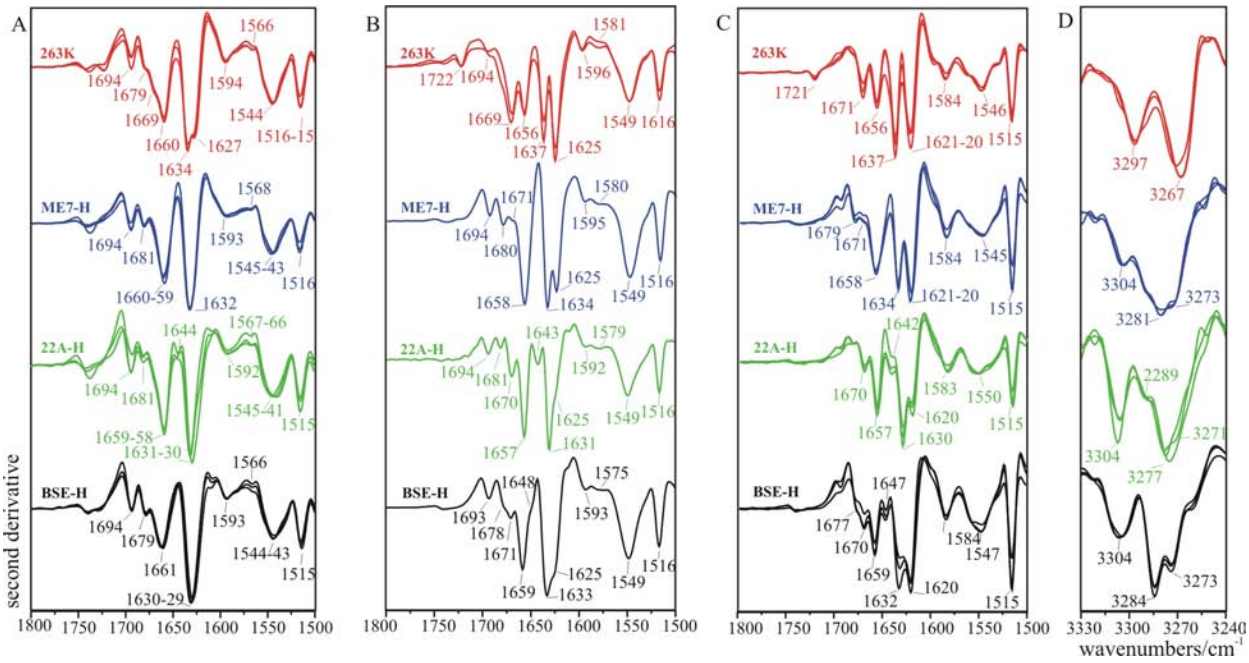

Figure 3.13 PrP27-30 second derivative spectra in the amide sensitive spectral ranges- amide I, amide II and amide A, obtained from different TSE strains A) dried samples B) H_2O suspensions C) D_2O suspensions. The spectra have been normalized between 1750 and 1600 wavenumbers and in the range 3330-3240 cm^{-1}, respectively. The overlaid spectra represent measurements of samples purified in independent extraction and purification procedures

spectra consistently exhibit specific infrared patterns for all four TSE strains, particularly in the secondary structure sensitive amide I region between 1600 -1700 cm^{-1}. The second derivative spectra of PrP27-30 from dried samples (Figure 3.13 A) show that all four TSE isolates are characterized between 1627 and 1637 cm^{-1} by intense low frequency β-sheetabsorption bands. The PrP27-30 samples fully hydrated in H_2O or D_2O (Figure 3.13 B and C) show two distinct β-sheet features between 1620 and 1637 cm^{-1}.The amide I band components between 1620 cm^{-1} and 1625 cm^{-1} can be assign to an intermolecularly hydrogen bound amide I >C=O groups in β-sheets (Caughey *et al.,* 1991b; Fabian *et al.,* 1993; Thomzig *et al.,* 2004). The components between 1630 and 1637 cm^{-1} most likely indicate peptide >C=O groups involved in intramolecular β-pleated sheet structures detected by infrared spectroscopy for many already known protein structures (Bandekar 1992; Barth *et al.,* 2002; Fabian *et al.,* 2002). The dried and the hydrated (in H_2O) samples of all isolates investigated constantly showed a weak band component around 1694 cm^{-1}, which is assign to the so-called high frequency component of antiparallel β-sheet pleated structures (Bandekar 1992; Barth *et al.,* 2002; Fabian *et al.,* 2002). Tentatively, the occurrence of band components at 1620 to 1625 cm^{-1} and around 1694 cm^{-1}, is assigned to intermolecularly formed antiparallel β-sheet structures in PrP27-30 (Caughey *et al.,* 1991b; Fabian *et al.,* 1993; Kubelka *et al.,* 2001; Thomzig *et al.,* 2004). All strains analysed show a very characteristic band component with

medium to strong intensity between 1656 and 1661 cm^{-1}, which is assign to α-helical structures (Goormaghtigh 1990; Tamm *et al.,* 1997). Similar band frequencies have been described for proteins with membrane-spanning α-helices (Susi *et al.,* 1983; Fabian *et al.,* 1993; Kubelka *et al.,* 2001; Sokolowski *et al.,* 2005). Natively folded protein- in contrast- shows an α-helical band at 1651 cm^{-1} (Sokolowski *et al.,* 2005). A varying number of weak band components found in the frequency range between 1669 and 1681 cm^{-1} most probably indicate different types of turns or loop structures (Bandekar 1992; Barth *et al.,* 2002; Fabian *et al.,* 2002). Weak absorption features are present between 1648 cm^{-1} and 1642 cm^{-1} for samples from strain 22A-H and the BSE-H isolate. The assignment of bands at these frequency positions to unordered structures as established for other proteins (Byler *et al.,* 1986; Goormaghtigh 1990) is questionable, since random coil structures usually exhibit very broad features, while the above mentioned components were relatively sharp.

All strains consistently show weak absorption features, most pronounced however, in the spectra of 263K, around 1721-1722 cm^{-1}, resulting from >C=O ester stretching vibrations of small amounts of ester linked lipids present in PrP27-30 (Klein *et al.,* 1998). In the amide II region, between 1500 and 1600 cm^{-1}, the PrP27-30 samples show three main absorption features in the ranges 1583-1596 cm^{-1}, 1541-1549 cm^{-1}, and 1515-1516 cm^{-1}. The main amide II feature between 1541 and 1549 cm^{-1} can be attributed to α-helix structures (Bandekar 1992; Fabian *et al.,* 2002). The absorption at 1515-1516 cm^{-1} is due to ring vibrations of the tyrosine side chain, and the component band at 1583-1596 cm^{-1} probably to COO^- asymmetric stretching vibration of aspartate or glutamate (Barth 2000).

3.2.3 PrP27-30 of dried samples

For all TSE isolates investigated here, the second derivative spectra of the dried PrP27-30 samples (Figure 3.13 A) exhibited specific low frequency β-sheet bands between 1634 and 1627 cm^{-1} at positions characteristic for each isolate (see Table 3.I). The β-sheet band of the 263K isolate showed a peak at 1634 cm^{-1} together with a weakly resolved shoulder at 1627 cm^{-1}. All isolates investigated showed a weak component at 1694 cm^{-1}. The characteristic α-helical band around 1660 cm^{-1} showed a relatively high intensity for the strains 263K, ME7-H and 22A-H, but is markedly lower in the spectra of BSE-H. Other absorption features common for all studied strains were observed at 1681 cm^{-1} for ME7-H and 22A-H, and at 1679 cm^{-1} for BSE-H and 263K, and are most probably due to turn structures. An individual absorption component were observed for 263K as a small, but consistent

shoulder at 1669 cm^{-1} (also probably due to turns) and for the strain 22A-H at 1644 cm^{-1}, which remains unassigned. The absorption range from 1600 to 1500 wavenumbers showed similar amide II and amino acids side chain absorption characteristics.

Table 3.I Assignment of amide I band components to the secondary structure of dried PrP27-30 samples purified from different TSEs

TSE strain	Structural component peak positions cm^{-1}				
	β-sheet (low frequency)	Unassigned structure	α- Helix	Turns	β-sheet (high frequency)
263K	1627 1634		1660	1669 1679	1694
ME7-H	1632		1660-59	1681	1694
22A-H	1631-30	1644	1659-58	1681	1694
BSE-H	1630-29		1661	1679	1694

The absorption range from 1600 to 1500 wavenumbers showed very similar amide II and amino acids side chain absorption characteristics. A slightly different spectral shape was present for the band component centred around 1594-1592 cm^{-1}. Some band components i.e. C=O stretching of lipids, α-helices in amide I and II regions, and β-sheets, showed slightly different frequencies and/ or intensities in the average spectra obtained from independently purified samples. As pointed out above (see section 2.4.1), these variations are probably dependent on the quality of the dried protein film spots.

3.2.4 Hydrated PrP27-30 samples

The level of detectable spectral differences depends on the hydration state of the samples. When hydrated, the PrP27-30 samples showed highly resolved spectral features. The spectral contrast between the different TSEs increased significantly in comparison to the variations observed among the strains from the dried protein samples.

3.2.4.1 PrP27-30 samples hydrated in H_2O

Figure 3.13 B showed the second derivative spectra of the four TSE isolates obtained from H_2O suspensions. The absorption features of the spectra are comparable to those obtained from the dried samples. However the fully hydrated PrP27-30 samples showed much better resolved spectral features. These spectra reveal a higher number of distinguishable turn features in the range between 1681 and 1669 cm^{-1}. In addition each of the isolates showed two well-resolved low frequency β-sheet absorption characteristics. An intense individual α-helical band component centred between 1659 and 1656 wavenumbers (Table 3.II), and a weak common component at 1694 cm^{-1} (1693 cm^{-1} in the spectra of BSE-H) were seen in all spectra, but with very low intensity in the spectra from 263K. The presence of intermolecular

hydrogen bonded β-sheet structure was indicated at 1625 cm^{-1} as an intense peak for 263K, well resolved peak for ME7-H and as a shoulder for 22A-H and BSE-H. For all isolates the presence of intramolecular β-sheet structures was indicated by a well defined individual band with characteristic peak positions at 1637 cm^{-1} for 263K, 1634 cm^{-1} for ME7-H, 1631 cm^{-1} for 22A-H and 1633 cm^{-1} for BSE-H. Typical but very weak absorption features were observed at 1643 cm^{-1} and 1648 cm^{-1} in the spectra of 22A-H and BSE-H, respectively.

Table 3.II Assignment of amide I band components to the secondary structure of PrP27-30 samples hydrated in H_2O

TSE strain	Structural component peak positions cm^{-1}						
	β-sheet (low frequency)		Unassigned structure	α- Helix	Turns		β-sheet (high frequency)
263K	1625	1637	-	1656	1669		1694
ME7-H	1625	1634	-	1658	1671	1680	1694
22A-H	1625	1631	1643	1657	1670	1681	1694
BSE-H	1626	1633	1648	1659	1671	1678	1694

The investigated in H_2O PrP27-30 samples show a high degree of similarity of the spectral patterns in the absorption region between 1600 and 1500 wavenumbers.

3.2.4.2 PrP27-30 hydrated in D_2O

All isolates investigated in D_2O (Figure 3.13 C) showed two intense low frequency β-sheet specific band components between 1637 and 1620 cm^{-1}. Common for all spectra were the peaks at 1621-1620 cm^{-1} and a second β-sheet component centred at wavenumbers typical for each of the isolates (1637 for 263K, 1634 for ME7-H7, 1632 for BSE-H and 1630 cm^{-1} for 22A-H, see Table 3.III). The individual intensity of the two β-sheet components was characteristic for all samples. For BSE-H the peak at 1632 cm^{-1} was generally present as a shoulder of the main component at 1620 cm^{-1}, and the peak at 1620 cm^{-1} appeared as an individual peak or a shoulder of the main component at 1630 cm^{-1} for 22A-H. The TSE strains 263K, BSE-H and 22A-H gave high frequency absorption bands at 1671 and 1670 cm^{-1}, assigned to turn structures. A similar peak was weakly indicated in the spectra of ME7-H at 1671 cm^{-1}. The ME7-H and BSE-H-samples showed weak absorption features between 1679 and 1677 cm^{-1}, tentatively assigned to the high frequency component of β-sheets and/or turn components.

All analyzed strains also showed an α-helical absorption band at a characteristic frequency and with varying relative intensity in the range between 1656-1658 wavenumbers. As with the samples in H_2O suspensions, PrP27-30 from BSE-H exhibited a weak absorption

band at 1647 cm^{-1} and from 22A-H an absorption feature at 1642 cm^{-1}.Obviously H/D exchange induced small band shifts of nearly all amide I band components depending on the

Table 3.III Assignment of amide I band components to the secondary structure of PrP27-30 samples hydrated in D_2O

TSE strain	Structural component peak positions cm^{-1}					
	β-sheet (low frequency)		Unassigned structure	α- Helix	Turns	Turns/β-sheet (high frequency)
263K	1620-21	1637	-	1656	1671	
ME7-H	1620-21	1634	-	1658	1671	1679
22A-H	1620	1630	1642	1657	1670	
BSE-H	1620	1632	1647	1659	1670	1677

type of the secondary structure involved. The intermolecular β-sheet band shifted downward to 1621-1620 cm^{-1} after 1 hour incubation in D_2O and enhanced additionally the differences between the β-sheet characteristics from the different strain specific PrP27-30 samples (see Figure 3.13 B and C). The intramolecular β-sheet band of 22A-H at 1631 cm^{-1} and BSE-H at 1633 cm^{-1} shifted by one wavenumber to 1630 cm^{-1} and 1632 cm^{-1}, respectively. No change in the intramolecular β-sheet band was observed in the spectra of strains 263K and ME7-H. Deuteration also does not affect the absorption frequency of the α-helix band at 1659-1656 cm^{-1}. The partial hydrogen-deuterium (H/D) exchange of the protein samples induced also shifts in the high frequency β-sheet components to positions, where they could no longer be separate from turn absorption bands. However, a residual absorption component with varying intensity at 1694 cm^{-1} was occasionally observed in the spectra from ME7-H, BSE-H, and 22A-H.

The amide II band can be used to monitor the hydrogen-deuterium exchange, thus providing substantial information on the structure and flexibility of proteins (Backmann *et al.*, 1996; Barth *et al.*, 2002; Fabian *et al.*, 2002). In D_2O only a broad residual amide II feature of unexchanged amide N-H functional groups could be located at a frequency position specific for each isolate (1645 cm^{-1} for ME7-H, 1546 cm^{-1} for 263K, 1547 cm^{-1} for BSE-H and at 1550 cm^{-1} for 22A-H) indicating those amide N-H protons which resisted H/D-exchange at ambient conditions and which are termed "persisting protons" in proteins (Backmann *et al.*, 1996). To some extent, strain-specific features were revealed in the frequency range between 1571 and 1523 cm^{-1}. The changes in the amide II absorption region are a direct result of partial H/D exchange. However, assessment of the extent of H/D exchange cannot be made easily based on the residual intensities in the amide II region, since IR bands arising from amino acid side-chain groups overlap with the amide II band components. The amide A band

(Figure 3.13 D) is the best and direct indicator for residual, nonexchanged N-H groups in proteins (Backmann *et al.,* 1996; Fabian *et al.,* 2000). The amide A band originates from the N-H stretching vibrations of the amide groups in proteins and its exact frequency depends on the strength of the hydrogen bond (Barth *et al.,* 2002). Thus, different residual bands in the amide A region directly indicate different structural components that resist H/D-exchange and are characterized by different hydrogen bonding patterns. Differences in the amide A band features after partial H/D-exchange suggest different accessibility of amide N-H-protons to H/D-exchange and thus indirectly indicate secondary structures with different flexibility and/or structural stability. The PrP27-30 samples investigated in D_2O-suspensions also showed TSEs specific infrared patterns in the amide A region. These variations were indicated by the characteristic number and relative intensities of the observed amide A components. The strains 263K and 22A-H showed two main peaks centred at 3297 cm^{-1} and 3267 cm^{-1} or at 3304 cm^{-1} and 3277 cm^{-1}. A small shoulder at 2289 cm^{-1} is detected for the 22A-H strain. The BSE-H isolate showed two intense bands at 3304 cm^{-1} and 3284 cm^{-1} together with a pronounced shoulder at 3273 cm^{-1}. In contrast, the amide A absorption features of ME7-H were characterized by a broad absorption band and a shoulder at 3304 cm^{-1}. The component at 3304 cm^{-1}, although with a different intensity, was present in the spectra of ME7-H, 22A-H and BSE-H, but was not found in the spectra of 263K.

Regardless of the strain specific spectral pattern observed in the amide A absorption region, the H/D exchange level calculated as a ratio between the area of the amide A and the area of the tyrosine band show a small difference in the H/D exchange levels between the TSE strains (Figure 3.14).

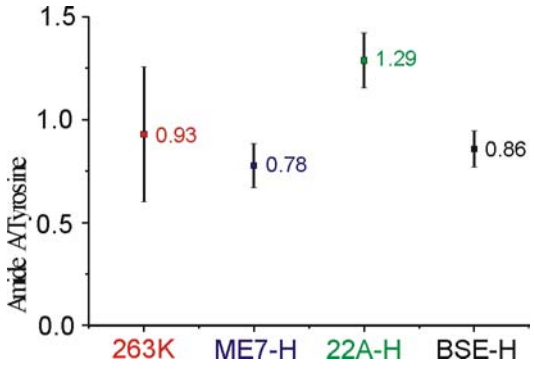

Figure 3.14 H/D exchange levels of the PrP27-30 from the four TSE strains obtained after 1 hour incubation in D_2O. The areas of the amide A (3330-3240 cm^{-1}) and Tyrosine (1523-1506 cm^{-1}) band components were calculated from the second derivative FT-IR spectra, which were not vector normalized.

However, the calculated average values, suggests that PrP27-30 from 22A-H shows slightly lower H/D exchange ratio followed by 263K and BSE-H and ME7-H, while the latter two show very similar H/D exchange ratios.

3.3 Cluster analysis

Cluster analysis was performed with the vector-normalized second derivative spectra using the Ward's algorithm and the Pearson's correlation coefficient for estimation of the spectral distances. The structural information contained in the amide A, I and II absorption regions of the dried protein spots, the H_2O- and D_2O-suspensions (as shown in Figure 3.13) was used as input data for hierarchical cluster analysis in order to obtain objective classification on the basis of the spectral patterns. The amide I of all FT-IR second derivative spectra obtained from dried or hydrated PrP27-30 samples contain specific absorption characteristics sufficient for proper strain discrimination (see Figure 3.15 A-D). However, the structural differences and the cluster density were found to depend on the hydrated state of the PrP27-30 aggregates. The dried samples showed lower structural differences between the TSE strains and considerable strain-internal structural variations (Figure 3.15 A). The hydrated samples showed significant strain dependent contrast (Figure 3.15 B and C). Especially the spectral information contained in the amide I and the amide A regions of PrP27-30 samples in D_2O was found to produce very distinct clustering. The classification schemes (Figure 3.15 C, D and E) obtained, respectively, on the basis of spectral information contained in the frequency ranges between 1619-1681 cm^{-1}, 3240-3330 cm^{-1} and 1528-1562 cm^{-1}, of samples in D_2O gave four dense and distinct spectral clusters, each including correctly the spectra obtained from PrP27-30 samples of the individual single strains purified in independent runs. The heterogeneity levels between spectra of independent measurements of a given strain were significantly lower than those between the different strain clusters. The dendrogram based on the amide I region suggested a higher spectral contrast between the different TSE strains than the one based on the amide A region. Furthermore, PrP27-30 isolated for the four TSE strains exhibited a clearly distinct structure from the protein content found in finally purified fractions from healthy hamster brains material (see Figure 3.15 D). Even the amide II region of the deuterated protein samples can be successfully used for strain differentiation by cluster analysis, since the broad band located at around 1547 cm^{-1} obviously also exhibit some strain specific features (Figure 3.15 F).

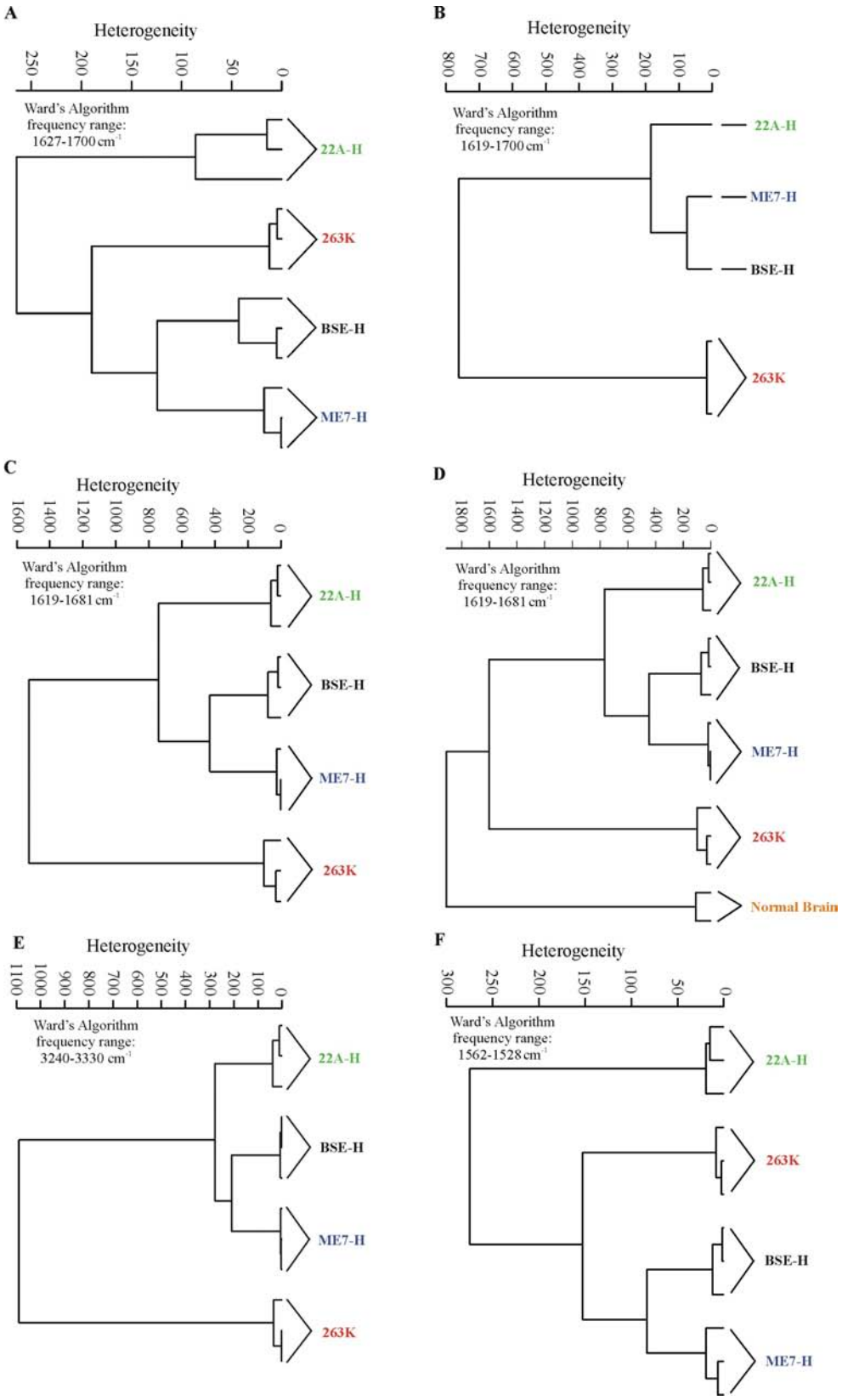

Figure 3.15 Dendrograms of a hierarchical cluster analysis show objectively the strain specific spectral diversity in the amide I of dried samples (A); samples hydrated in H_2O (B) or D_2O (C and D) and in the amide II (E) and amide A (F) of samples suspended in D_2O. Cluster analysis was performed with the vector-normalized second derivative spectra.

FT-IR studies of hamster adapted TSE strains (Caughey *et al.*, 1998; Thomzig *et al.*, 2004), suggested the intramolecular β-sheet band component as the most prominent indicator of strain identity. Indeed hierarchical cluster analysis of spectra obtained from D_2O suspensions reveal that the spectral characteristics of the intramolecular band component are, all by themselves, sufficient for the discrimination of the four TSEs (Figure 3.16)

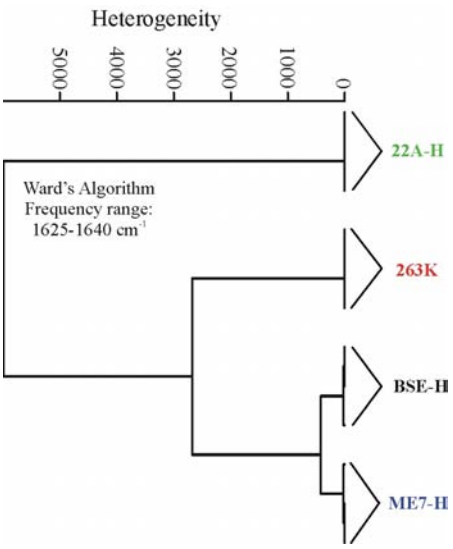

Figure 3.16 Hierarchical cluster analysis of TSE strains on the base of a single secondary structure component.

In the present work, the infrared spectra of ME7-H, 22A-H and BSE-H (three independent runs each) were obtained from PrP27-30 samples extracted and purified from different TSEs agents in Syrian hamsters (section 2.1.1). The spectral variations, objectively assessed by multivariate cluster analysis, showed that the structural characteristics of PrP27-30 samples obtained from different passages are indeed quite similar yielding dense strain clusters as indicated by the dendrograms given in Figure 3.15 and Figure 3.16). These results suggest a stable propagation of PrP^{Sc} secondary structure during passaging of the TSE strains.

3.4 Temperature gradient experiments

3.4.1 Temperature dependent structural changes of PrP27-30 from different TSEs

For many proteins (Backmann *et al.*, 1996; Fabian *et al.*, 2002), even long time periods of incubation of PrP27-30 samples in D_2O at room temperature results in incomplete H/D exchange of the amide protons as it can be seen from the residual amide A and amide II

band components (as described in section 3.2.4.2). The results from a 14 hours incubation of PrP27-30 in D_2O, to give an example, show only small additional H/D exchange in comparison to only one hour incubation, and consequently, only minor spectral changes in the amide A, I and II absorption regions can be seen (denoted by asterisks in Figure 3.17 A-D).

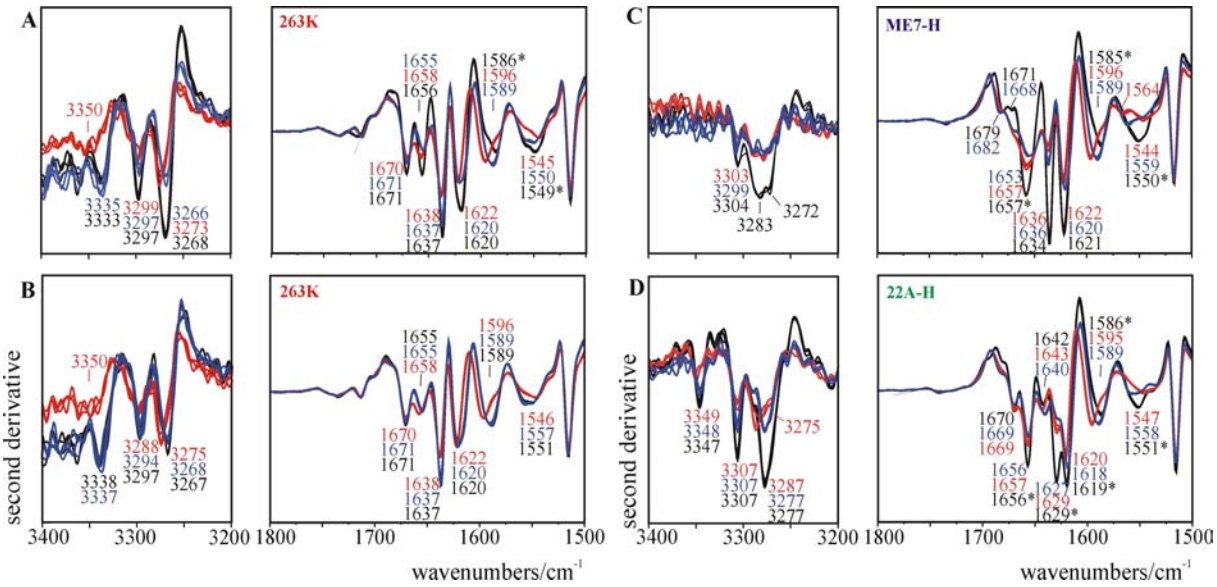

Figure 3.17 Temperature dependent changes between 20 and 90°C observed in the amide I, amide II and amide A spectral regions. First "thermo-cycle" applied to strain 263K (A), second "thermo-cycle" of strain 263K (B); first "thermo-cycles" applied to strain ME7-H (C) and to strain 22A-H (D). The black spectra were obtained at the beginning of the temperature gradient measurements, starting from 20°C, the red spectra were obtained at the end of the upward temperature gradient ending at 90°C, and the blue spectra at the end of the downward gradient ending at 20°C. Compared to an 1 hour H/D exchange of the samples prior to FT-IR measurements (see Figure 3.13 C and D) a 14 hours H/D exchange yielded only small spectral variations (see bands marked with asterisks).

The slightly changed amide I bands do not affect the strain-specific internal heterogeneity levels as proven by the multivariate cluster analysis shown in Figure 3.18.

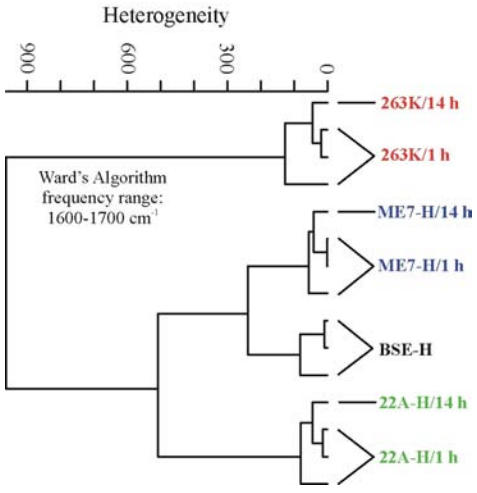

Figure 3.18 Hierarchical cluster analysis of PrP27-30 samples obtained after 1 or 14 hours of incubation in D_2O.

These findings clearly suggest that most of the H/D exchange of the prion rods is already achieved at room temperature within the first hour in D_2O. Significant spectral changes, however, were observed, when the PrP27-30 samples in D_2O were heated up to 90°C (Figure 3.17 A, C, D). These changes are due to deuteration of residual peptide backbone N-H groups which persisted H/D-exchange at room temperature and to temperature induced conformational transitions. Common for all strains was the irreversible intensity decrease of the amide A and II band components due to this "residual" H/D exchange. Concomitantly, the spectra showed intensity degrease of nearly all secondary structure components as a function of increasing temperature. The FT-IR spectra of the three TSE strains showed that even after increasing the temperature up to 90°C a considerable amount of secondary structure retained and parts of the structural changes are reversible.

Additionally, all strains exhibited a very peculiar band narrowing and a band shift to higher frequencies of the intermolecular β-sheet component from approximately 1620 to 1622 cm^{-1} at 90^{o}C (see Figure 3.17 A, C, and D). The latter spectroscopic behaviour could be due to the presence of two different types of intermolecular β-sheet structures that overlap to one single unresolved band at room temperature but differ in thermal stability, with the lower frequency component at 1622 cm^{1} being thermo-stable. Two intermolecular β-sheet components were already observed in the dilution experiments performed with PrP27-30 from 263K (see section 3.1.5). The temperature gradient measurements revealed strain specific changes in the amide I, II and A absorption regions (Figure 3.17 A, C and D). In general, the temperature induced changes in the spectra of ME7-H were significantly larger than those of 263K or 22A-H. Also the temperature-induced 'residual' H/D-exchange in PrP27-30 from ME7-H, but not from 263K and 22A-H, was almost complete at the end of the first temperature cycle as indicated by the significant intensity changes of all amide A band components and the amide II band at 1550 cm^{-1}. The temperature treatment at 90^{o}C did not affect the secondary structure "fingerprint" of 263K, whereas the corresponding secondary structure components of ME7-H and 22A-H, e.g. turns and intramolecular β-sheets, were dramatically changed. Furthermore, the temperature gradient measurements revealed that each strain was characterized by a strain-specific thermoresistance as indicated by the transition curves of the three secondary structure elements shown in Figure 3.19. The resulting curves showed (i) non-cooperative transitions of the secondary structures for all TSE strains but (ii) a strain specific thermo-resistance of particular secondary structure.

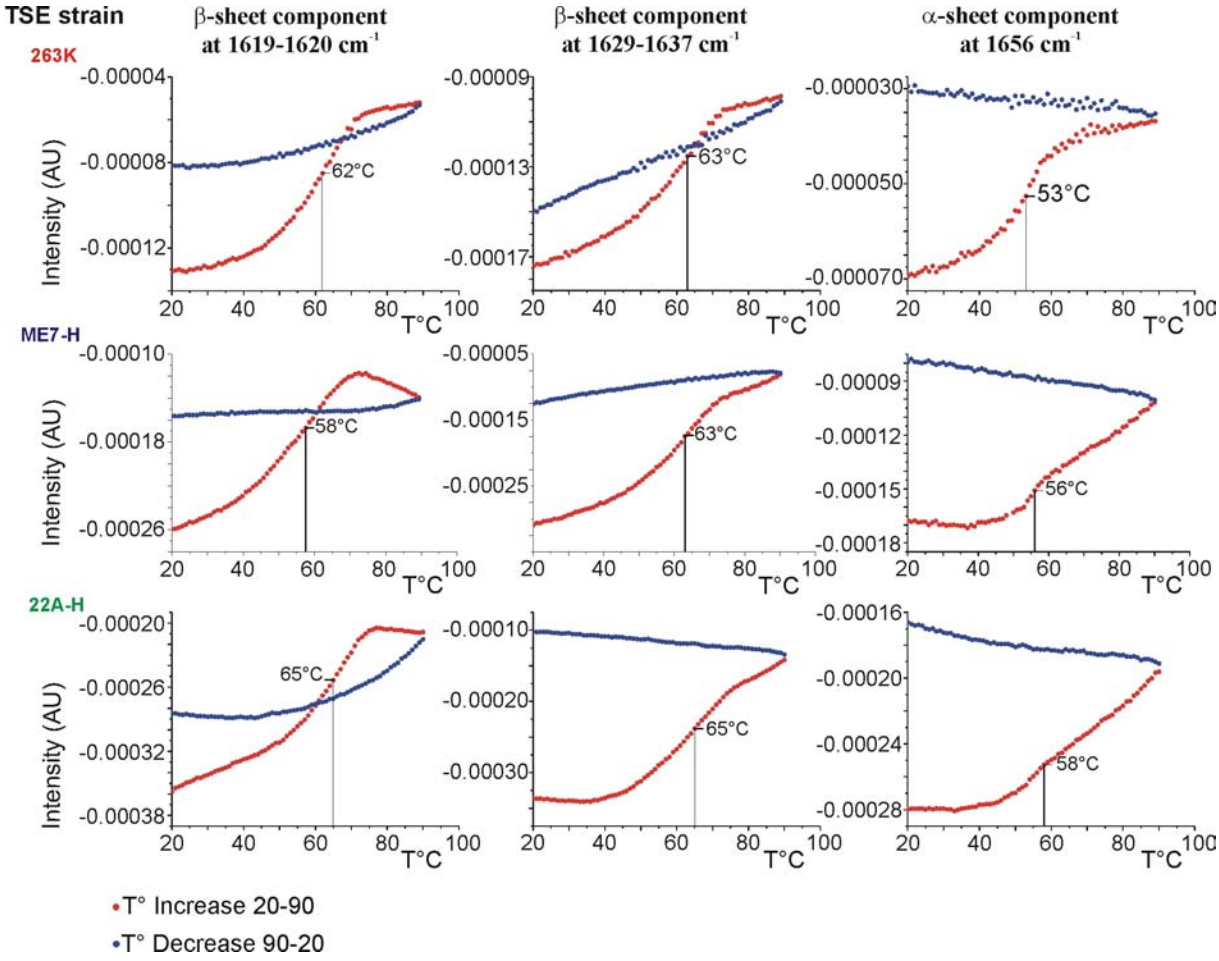

Figure 3.19 Strain specific and secondary structure dependent transitions followed by the intensity changes of some pronounced amide I band components during the first heating (red points) and cooling (blue points) thermo-cycles. The temperature where the band components showed highest intensity changes was evaluated from the first derivative $dI / dT°C(a.u.)$ transition curve maximum calculated using a 9 smoothing point function (using Origin 6.1 software).

A second thermo-cycle applied to the samples of 263K (see Figure 3.17 B) do not lead to further H/D-exchange and irreversible changes of the protein structure. However, the second thermo-cycle clearly showed the reversible frequency shifts and intensity changes of amide I, II and A bands during the heating and cooling thermo-cycles, with the unique reversible band sharpening of the β-sheet band at 1620 cm^{-1} being particularly interesting. The reversible changes induced by high temperature during the second thermo-cycle revealed a certain co-relation between the behaviour of the amide I and the residual amide A band components in response to the temperature changes. The amide A component at 3267 cm^{-1} in the spectra of 263K showed narrowing and shift to higher frequencies at 90°C, as characteristic for the intermolecular β-sheet band at 1620 cm^{-1}. The components at 3297 and 3338 cm^{-1} showed a high frequency shift and broadening with increase of the temperature, in

the same way as the intramolecular β-sheet and α-helical band components at 1637 and 1665 cm^{-1}, respectively. However, an assignment of the observed amide A band components to protein secondary structures on the basis of changes in these spectral characteristics remain speculative.

Hierarchical cluster analysis of all spectra collected from the three TSE strains during the temperature gradient measurements result in a dendrogram, composed of three main clusters each including all spectra obtained from the corresponding strain at any temperature between 20°C and 90°C (Figure 3.20). Consistent with the strain-specific differences observed from samples suspended in D_2O at room temperature (Figure 3.15 C), the secondary structure of strains ME7-H and 22A-H differ significantly from that of 263K at all temperatures. Each strain specific cluster shows the spectra correctly ordered according to the temperature increase and is characterized by distinct sub-clusters with class-internal heterogeneity levels, objectively reflecting the degree of the strain specific structural changes induced by the temperature treatment.

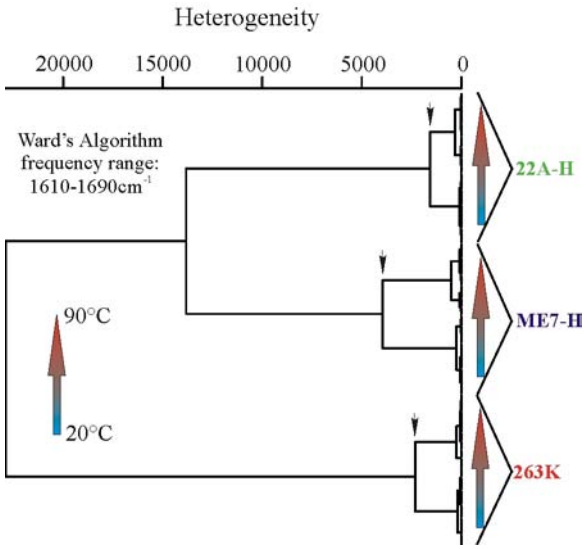

Figure 3.20 Dendrogram of hierarchical clustering showing specific thermal stability of PrP27-30 samples from different TSEs, expressed by the different strain internal heterogeneity levels (designated by arrows).

This sub-clustering scheme clearly shows that ME7-H undergoes the largest, 263K intermediate and 22A-H the smallest overall structural alterations as a function of temperature. At the same time the three strain-specific classes show an individual sub-clustering scheme, which reflect objectively the strain-specific temperature response.

3.4.2 FT-IR characteristics of the PK resistant fraction of heated PrP27-30 samples

High temperature treatment of scrapie-infected brain homogenates induces reconstitution of the sensitivity to PK digestion of the PrP27-30 molecules as described elsewhere (Somerville *et al.,* 2002). Western blot analysis of PrP27-30 samples from strain 263K heated at 90°C and subsequently digested with PK (Figure 3.21) show that a considerable amount of PrP molecules have altered properties in respect to the specific detection of the PrP27-30 by the 3F4 mAb (lane 1), whereas no significant differences are seen between heated, but not additionally digested samples (lane 2) and the controls, which either had not been heated, but additionally PK-digested (lane 3), or not heated and PK digested (lane 4). Lane 5 shows PK-digested brain homogenate diluted by a factor of 10^{-6} as a control. As suggested by lanes 1-4, the glycosylation profiles of all samples are identical with the glycosylation pattern of PK digested scrapie brain homogenate (lane 5), indicating that high temperature do not change the glycosylation profile of the PrP27-30 molecules.

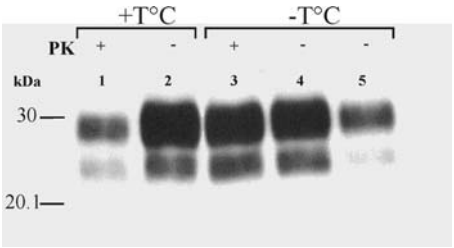

Figure 3.21 Temperature induced PK sensitivity of PrP27-30 from scrapie strain 263K. Samples characterized by western blotting of PrP27-30 with 3F4 mAb. Lane 1- Heat treated and subsequently PK digested samples. Lane-2 Control sample, heat treated sample, no additional PK-digestion. Lane-3 Control, no heat-, but additional PK-treatment. Lane-4 Control, no heat- and no additional PK-treatment. Lanes 1-4 represent ~0.75 ng PrP27-30 (starting material). Lane-5 represents PK digested scrapie brain homogenate diluted by a factor of 10^{6} as a control to monitor the qualitative state of the samples (0.1 ng PrP27-30).

FT-IR spectra of heated and subsequently PK-digested 263K PrP27-30 samples, hydrated in D_2O for IR spectroscopy (Figure 3.22, red spectrum) show a slightly different spectral pattern in comparison with the untreated sample (Figure 3.22, black spectrum). The temperature and PK treated prion aggregates exhibit smaller intramolecular β-sheet absorption in comparison to the intact PrP27-30 aggregates. At the same time the intramolecular β-sheet band also slightly shifts to 1638 cm^{-1} and the turn specific band component to 1672 cm^{-1}.

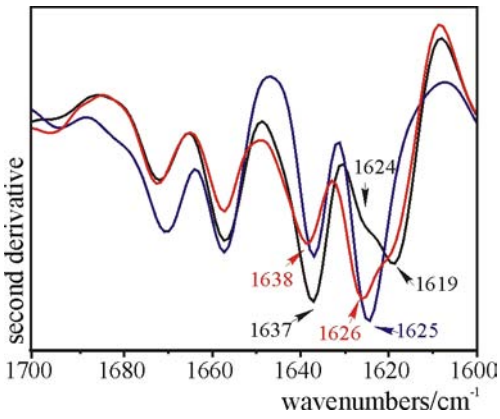

Figure 3.22 FT-IR spectra of PrP27-30 from strain 263K in D_2O after heat treatment and subsequent PK digestion (red spectrum) compared to the control spectrum obtained from untreated PrP27-30 samples in D_2O (black spectrum) and H_2O (blue spectrum). For graphical representation the second derivatives were vector-normalized between 1750 and 1600 wavenumbers.

The characteristic of the intermolecular β-sheet band seen in the treated samples was quite intriguing: After heating of PrP27-30 and subsequent digestion of the PK sensitive part of the aggregates, this β-sheet component was centred at 1626 cm^{-1} and was characterised by a weak shoulder at about 1619 cm^{-1}, whereas the peak maximum of untreated PrP27-30 samples was located at 1619 cm^{-1} together with a shoulder at 1624 cm^{-1}. The low frequency β-sheet bands at 1638 cm^{-1} and at 1626 cm^{-1}, respectively, in the PrP27-30 samples after temperature treatment and consequent PK digestion showed a notable similarity to untreated samples hydrated in H_2O (Figure 3.22, blue spectrum).

FT-IR microscopic measurements of the dried PrP27-30 samples enabled us to collect easily spectra in the mid-infrared spectral region between 4000 and 800 cm^{-1}. This spectral region contains characteristic infrared bands originating from different types of functional groups from various macromolecules (figure 7, black curve). The most intensive IR absorption bands of all PrP27-30 samples were generally the protein amide I and amide II bands. However absorption patterns characteristic for other functional groups are also present in the spectra of PrP27-30 samples: The region between 3000 and 2800 cm^{-1}, is dominated by the CH_2 and CH_3 stretching vibrations of the fatty acids chains in lipids and the spectral range between 1200 and 800 cm^{-1}, is dominated by the complex absorption features of carbohydrates (see Table 1.IV)

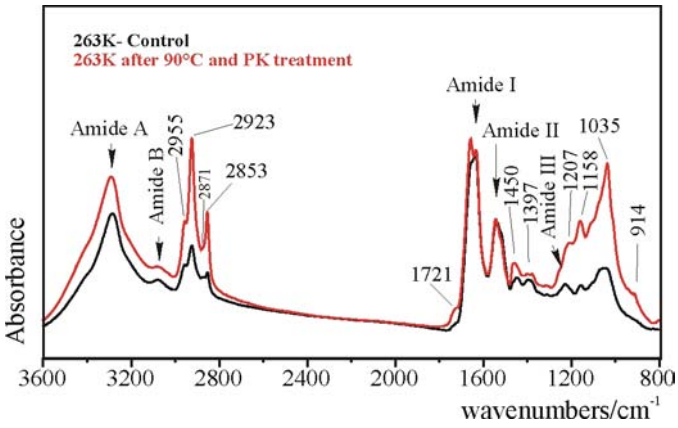

Figure 3.23 Spectral comparison of heat- and PK treated (red spectrum) and untreated (black spectrum) PrP27-30 samples. The spectra represent an average of three independent PrP27-30 film spot measurements of heat treated and subsequently PK-digested samples, and control samples from 263K. The spectra have been vector-normalized in the amide I region.

PrP^{Sc} is glycosylated with a set of complex bi, tri, and tetraantennary, N-linked oligosaccharides that also contain sialic acid (Rudd *et al.*, 1999). Moreover lipids and specific carbohydrate polymer were found to be associated with the scrapie fibrils (Klein *et al.*, 1998; Appel *et al.*, 1999), and also small amounts of host-specific nucleic acids were constantly co-purified within the PrP27-30 preparations (Kellings *et al.*, 1992; Diringer *et al.*, 1997). FT-IR spectra obtained from the temperature treated and consequently PK digested PrP27-30 samples, show striking differences between the relative amount of proteins, lipids, and carbohydrates, as demonstrated by the spectra, (Figure 3.23, red curve) in comparison to the untreated samples (Figure 3.23, black curve). This result suggests a possible protective function of the non protein components in the PrP27-30 aggregates from 263K scrapie strain.

3.5 Kinetic measurements of ^{13}C Urea induced unfolding of PrP27-30 from 263K

The second derivative FT-IR spectra obtained during the time course of urea induced PrP27-30 secondary structure transitions showed characteristic time dependence (Figure 3.24). Half an hour after being suspended in 6M urea solution, the amide I absorption bands still show absorption features typical for the 263K strain, β-sheet bands at 1637 and 1620 cm^{-1}, α-helices at 1656 and turn absorptions band components at 1671 cm^{-1}. With the time the intensity of all secondary structure band components decrease. The intermolecular β-sheet band shows characteristic changes as revealing of a shoulder at 1624 cm^{-1} and a shift of the main component to lower frequency.

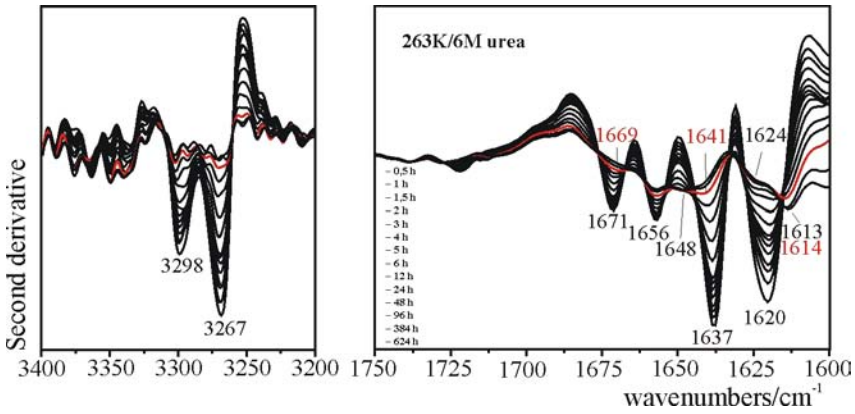

Figure 3.24 Time course of the secondary structure changes of PrP27-30 in the presence of 6M urea.

The intramolecular β-sheet absorption at 1637 cm^{-1} shows a pronounce intensity decrease and a shift to higher frequency. The turn absorption band at 1671 cm^{-1} is undetectable at the end of the measurements. The α-helix at 1656 cm^{-1} shows intensity changes but no shift in its absorption position. This component also remains detectable after incubation for 624 hours (26 days) in 6M urea. The decrease of the intensity and the broadening of the original band components, as well as the raised peak at 1648 cm^{-1}, indicate predominantly disordered state of PrP27-30 at the end of the measurements, or the prolonged incubation in 6 M urea led to unfolding/denaturation of the main part of the aggregates in the sample. The amide A intensity changes show that nearly complete H/D exchange is achieved after exposure of the sample for 8 days (192 hours) to the denaturant (see the red curve in Figure 3.24). However, characteristic secondary structure components like the α-helix at 1656 cm^{-1} and the intermolecular β-sheet band with a main peak at 1613 cm^{-1} and a shoulder at about 1624 cm^{-1} were still present in the spectra even 26 days after the incubation in 6 M urea, indicating the presence of persisting protein aggregates in the sample.

The data points of the time dependent intensity changes of the pronounced amide I and A components (shown in Figure 3.24), each typical for a given secondary structure, were fitted using a basic sigmoidal function (from "Origin 6.1" software, see equation 1) see (Figure 3.25).

$$y = \frac{A_1 + A_2}{1 + (x / x_0)^p} + A_2 \qquad \textbf{Eq. 3.1}$$

where the fitting parameters A_1, A_2, x_0 and p were initial, final, center values and power, respectively.

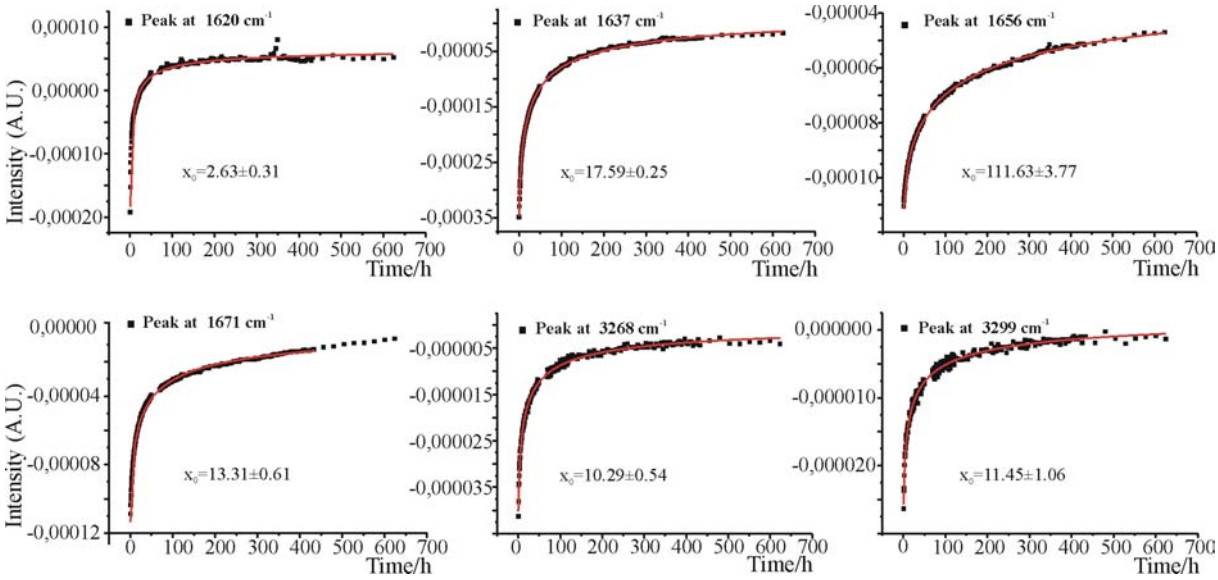

Figure 3.25 Time dependent secondary structure transitions in the PrP27-30 samples exposed to 6M urea

Sigmoidal data points distribution suggest a simple two-state transition process from folded to unfolded state (Barth *et al.*, 2002). However, each secondary structure component shows individual transition characteristics, suggesting non-cooperative unfolding of the PrP27-30 aggregates in the presence of 6M urea.

3.6 Discrimination of sCJD disease and its strains from blinded human brain samples

The successful discrimination of hamster adapted TSEs by means of FT-IR spectroscopy of purified PrP27-30 samples, gave a green light to explore the differentiation capacity of the FT-IR spectroscopy technique also for human prion diseases and the strains involved. 27 human brain samples from sporadic CJD (sCJD) patients and controls (see section 2.1.2) were examined in a blind experiment in regard to the individual cases. Each sample was obtained at autopsy from the frontal cortex, which is a region abundant of PrP^{Sc} in CJD patients (Parchi *et al.*, 1997; Hill *et al.*, 2003).

3.6.1 Extraction and purification of PrP27-30

Unlike the hamster brain homogenates, which produced clear brown-stained supernatants (S_{16}) after the first centrifugation (15 min at 16 000g), the centrifuged 10% human brain homogenates exhibited varying turbidity and different nuances of yellow. This difference was possibly due to variations in the proportions between the white and the gray matter in the dissected brain tissue. The human brain sample Bn116 showed the most unusual S_{16} supernatant with an untypical contaminant, probably lipid material that was distributed from top to bottom in the vial as a dark stained column. Such contamination was not observed for sample Bn116a, although it originated from the same human donor, indicating variations in the chemical composition of adjacent pieces from the frontal cortex of a single human brain. The pellet of all brain specimens after the final centrifugation contained PK-resistant protein fractions both in sCJD and control brain tissue samples. The total amount of the purified protein varied in a wide range of 5.4-39 µg/BE (see Appendix 3)

3.6.1.1 Silver staining properties of PK resistant fractions purified from human samples

The SDS-PAGE followed by silver staining (Figure 3.26) showed samples with varying protein content and no staining for the PrP27-30. Only very weak shadows in the regions corresponding to the expected molecular weights between 19 and 30 kDa were seen (see black arrows, Bn116, gel A and gel H; Bn128, gel B).

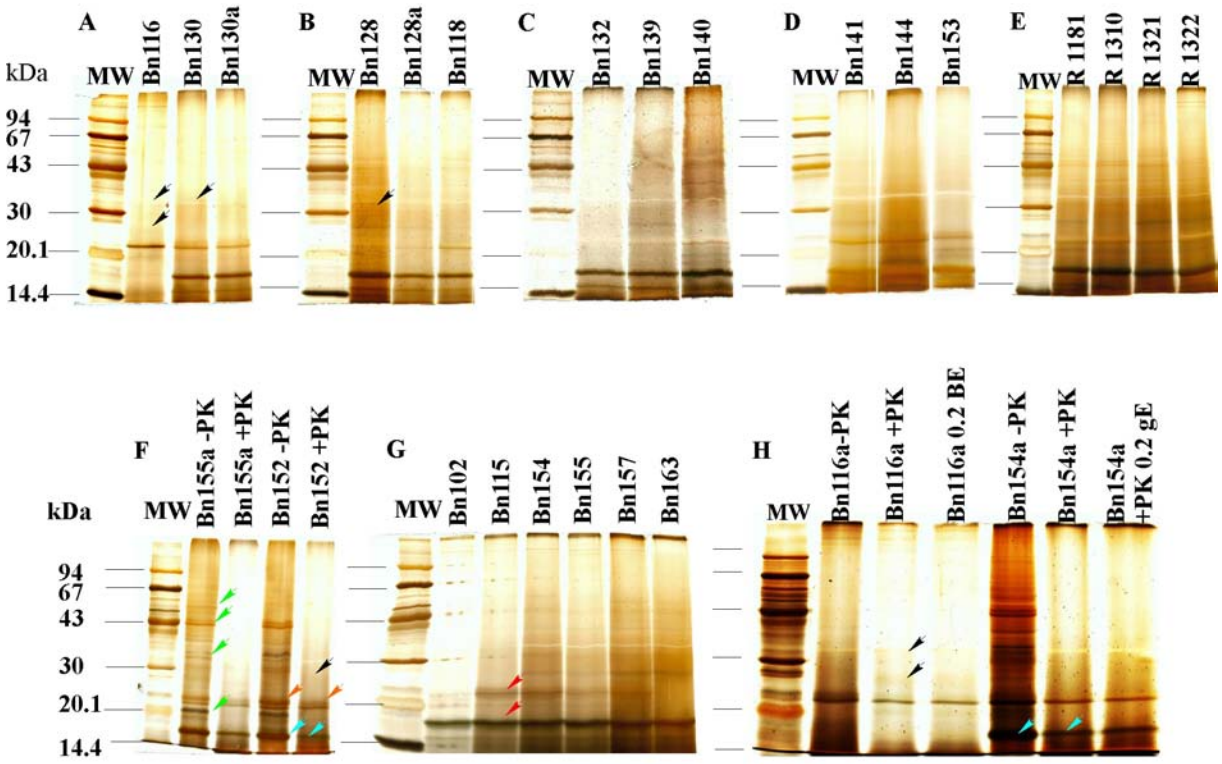

Figure 3.26 SDS-PAGE followed by silver staining of the protein samples extracted and purified from human brain material. The samples represent 0.1 BE of PK treated proteins, unless indicated otherwise. For estimation of the efficiency of the PK treatment, some samples were assayed before (-PK) and after PK treatment (+PK).

However, similar staining was present in samples, that do not show specific immunostaining with the 3F4 mAb, or presumably were from non-CJD patients (see black arrows, Bn130 gel A; Bn152 gel F). Most of the samples showed an intensively stained band at 16-17 kDa and staining at about 20 kDa (red arrows, Bn115, gel G; Fig.) similar to the hamster PrP27-30 preparations (see section 3.1.1).The light and heavy chains of human ferritin have molecular weights of 20.021 kDa and 22.179 kDa, respectively (Peri 2003). Ferritin has been demonstrated to be major contaminant in hamster PrP27-30 preparations (Diringer et al., 1997). Therefore, the single or double bands observed at ~20 kDa with varying intensity were most probably due to the presence of ferritin in the human PrP27-30 preparations. Samples not treated with PK also show specific staining at ~20 kDa also probably due to ferritin, intense staining at ~17 kDa and a variety of high and low molecular weight silver-stained bands, which are not detectible after PK treatment (green arrows, Bn155a -/+PK, gel F,). It should be noted that the band at about 17 kDa is significantly reduced after the PK treatment (blue arrows, Bn152 -/+PK, gel F; Bn154a -/+ PK gel H, Figure 3.26), whereas ferritin remained nearly unaffected (orange arrows, Bn152 -/+PK gel F,). Interestingly, clear PrP^{Sc} bands were not seen in CJD samples before PK treatment.

FT-IR spectra obtained before and after PK treatment showed that unlike the PrP27-30 preparation from 263K (see section 3.1.6.) the second derivative spectral characteristic of human samples treated or not treated with PK differed dramatically in respect to the aggregation specific bands of the proteins in the sample (Figure 3.27).

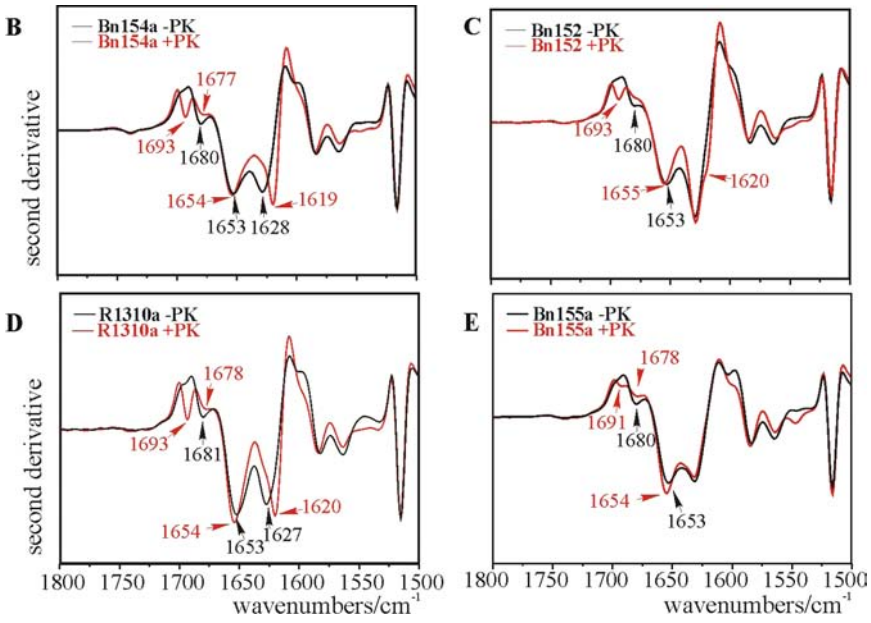

Figure 3.27 FT-IR second derivative absorption spectra of samples before and after treatment with PK

Indeed, band components indicative for the presence of aggregated proteins are clearly seen only after enzyme digestion (see absorption band components at 1693 and 1619-1620 cm^{-1}). However, similar characteristics of aggregated proteins band components were found in non-CJD control samples (Figure 3.27 C and D). Interestingly, sample Bn155a (Figure 3.27 E) do not show any significant absorption features indicative for aggregates although it originated from a CJD diseased donor, as revealed latter on (see Table 3.IV).

3.6.1.2 Immunostaining with 3F4 mAb

SDS-PAGEs followed by Western blotting and immunostaining with 3F4 mAb, showed eight negative samples from six patients. No PrP27-30 was detected with 3F4 mAb in the final protein pellets of samples Bn130, Bn130a, Bn140, Bn152, Bn153, Bn115, R1310 and R1310a. The rest (19 samples from 15 patients) showed three bands characteristic for PrP^{Sc} representing diglycosylated, monoglycosylated and unglycosylated forms of the prion molecules. The specific electrophoretic mobility of PrP27-30 creates a glycosylation pattern, which is used for the discrimination of type 1 and type 2 PrP^{Sc} in sporadic CJD cases according to the electrophoretic mobility of the unglycosylated PrP molecules; 21 kDa and 19 kDa, respectively (Parchi *et al.*, 1996; Parchi *et al.*, 1997). The investigated samples

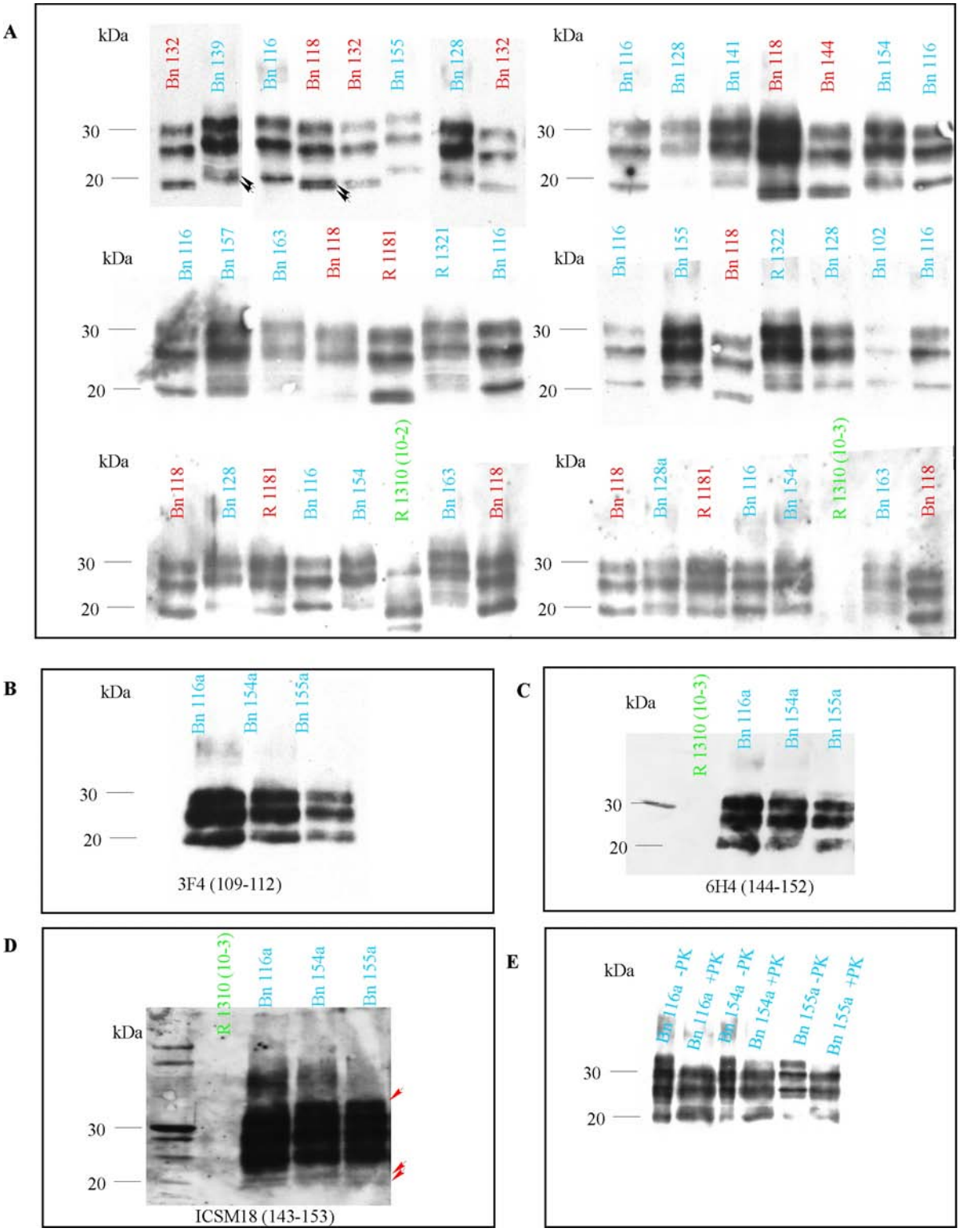

Figure 3.28 SDS-PAGE followed by western blotting and immunostaining with 3F4 mAb (panels A, B and E), 6H4 (panel C) and ICSM18 mAbs (panel D). Panel E showed the quality state of the PrPSc and PrP27-30 samples before and after treatment with PK, respectively. Samples represented 10^{-4} BE (unless indicated otherwise). Green labels- non-CJD samples / Blue labels- type 1 PrP^{Sc} / Red labels- type 2 PrP^{Sc}

Table 3.IV Human samples information

Sample designation	Sample Weight /g	purified protein µg/g brain	Codon 129 Polymorphism*	Lab-internal PrP^{Sc} typing	Lab-external PrP^{Sc} typing*	Diagnosis*
BN102	4.8	15	MM	1	1	CJD long disease duration
BN115	5.3	19.2	missing	-	negative	multiple infarction
BN116	4.9	5.4	MM	1	1	CJD long disease duration
BN116a	2.5	7.9	MM	1	1	CJD long disease duration
BN118	5.25	7.2	MV	2	2	CJD
BN128	5.3	12,8	MM	1	2	CJD
BN128a	4.78	14.3	MM	1	2	CJD
BN130	5.02	11	missing	-	negative	amyotrophic lateral sclerosis (ALS)
BN130a	4.85	12,2	missing	-	negative	ALS
BN132	5.06	7	MM	2	?	
BN139	4.5	7.2	MM	1	1	CJD, cerebellum negative
BN140	4.01	18.25	missing	-	negative	CJD
BN141	4.57	20	questionable	1	1	presenil Alzheimer disease
BN144	5.05	18.8	MV	2	2	CJD
BN152	5.2	28.5	missing	-	missing	CJD
BN153	5.35	39.8	missing	-	negative	missing
BN154	4,7	20.1	MM	1	1	dementia with Lewy Bodies (DLB)
BN154a	5.3	28.2	MM	1	1	CJD long disease duration
BN155	4,5	14.6	MM	1	pending	CJD long disease duration
BN155a	5.2	16.7	MM	1	pending	CJD
BN157	4,8	36,4	pending	1	pending	CJD
BN163	6,7	18.,6	pending	1	pending	-
R1181	3.4	19.4	VV	2	1	CJD
R1310	4.5	29	missing	-	negative	white matter disease
R1310a	4.9	31.8	missing	-	negative	white matter disease
R1321	4.3	26.2	MM	1	1	CJD
R1322	4.1	36	MM	1	1	CJD

* Data supplied by the sample provider

Green labels- non-CJD samples / Blue labels- type 1 PrP^{Sc} / Red labels- type 2 PrP^{Sc}

As seen from the table, samples R1181, Bn128 and 128a, have been controversially classified.

showed variations in the molecular weight of the lower PrP band, which enabled a tentative assignment of the samples to PrP^{Sc} type 1 or 2 (see Figure 3.28, Table 3.IV). However, the Western blots revealed some subtle variations in the glycosylation patterns, in respect to the band intensities and migration patterns of the three PrP glycoforms. The sample R1310 showed a single diffuse shadow at ~20 kDa, when 10^{-3} BE was analyzed. Since no other negatively stained sample showed similar staining properties, an aliquot representing 10^{-2} BE from R1310 was assayed. It shows intensively stained bands at about 25, 19 and 17 kDa, which differed from the characteristic staining pattern of PrP27-30 with 3F4 mAb. Therefore, the sample was considered as CJD negative. No such staining was found in a sample purified in an independent run of brain material from the same donor (sample R1310a), suggesting the presence of unspecifically stained contamination proteins, present in higher amounts in the first sample analyzed.

Immunostaining with 6H4 (Figure 3.28) and ICSM18 mAbs (Figure 3.28 D) revealed higher sensitivity of the ICSM18 mAb. In this assay additional PrP bands stained at ~35-33 kDa were seen (detectible as shadows after staining with 6H4 or 3F4 mAbs) and some bands between 18-16 kDa (designated by red arrows, Figure 3.28). Similar bands were not found in Western blots of similarly diluted samples stained with 6H4 or 3F4 mAbs.The ICSM18 mAb revealed additional differences between the three CJD positive samples. The samples Bn154a and Bn155a showed more intensively stained bands at ~35-33kDa than Bn116a. Sample Bn116 showed two distinct bands of ~19 and ~18 kDa, sample Bn154a had a diffuse band at ~19 kDa and the sample Bn155a showed two diffuse bands at ~18 and ~17 kDa. The staining at ~35-33 kDa is certainly due to the presence of intact PrP^{Sc} molecules, whereas the 19-17 kDa bands were probably indicative for the existence of different truncated forms of glycosylated and unglycosylated PrP molecules. Furthermore, some of the investigated samples (i.e. Bn139, Bn118, Figure 3.28 A) showed more or less clear splitting of the unglycosylated PrP band (at 19-21 kDa) after staining with 3F4 mAb (see black arrows, Figure 3.28). The differences between samples Bn116 and Bn154, both from patients homozygous for methionine at codon 129 and disease characterized by a prolonged clinical duration (see Table 3.IV), implicate that distinct strains or PrP conformers could be associated with a similar disease phenotype, or that a factor other than PrP could be responsible for some of the disease characteristics. Immunostaining of samples not treated with PK (Figure 3.28 E) showed four PrP^{Sc} bands at ~35-33, 30, 25 and ~20 kDa, most probably due to the presence of already truncated PrP^{Sc} molecules in the human brains as a result of autoproteolysis.

3.6.1.3 FT-IR characteristics of the protein samples

In all investigated samples the protein content was sufficient for the generation of FT-IR spectra. The absorption spectra obtained (in D_2O suspensions), showed intense amide I and residual amide II absorption bands as exemplarily shown in Figure 3.29. The Amide I maximum of the protein absorption spectra of the human samples were located in a broad range between 1631 and 1653 wavenumbers (see Table3.V), suggesting the predomination of different secondary structures among the investigated human samples.

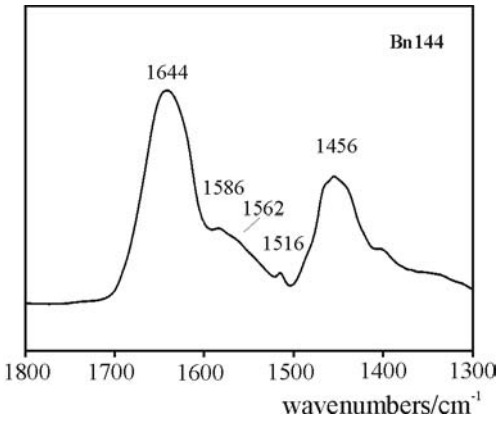

Figure 3.29 Typical absorption spectrum obtained from D_2O suspended PK resistant fractions from human brain tissue

A residual amide II band component was observed in the range between 1565 and 1560 cm^{-1}. The spectral characteristics of amide II indicate that most of the samples had nearly the same H/D exchange levels, except samples Bn102 and Bn116, which showed a slightly stronger amide II band absorption at 1565 and 1564 cm^{-1} (see Appendix 3)

3.6.1.4 Secondary structure analysis from the second derivative FT-IR spectra

The second derivative FT-IR spectra from all 27 samples (from 21 human donors) showed proteins with two more or less clearly distinct two low frequency β-sheet and an α-helical component (see Figure 3.30), as well as small contributions from turns and probably high frequency β-sheet bands (see Table 3.V). In the spectra of Bn102 and Bn116 (Bn116a), C=O stretching band components characteristic for lipids were present at 1738 and 1739 cm^{-1}. Bands from C=O stretching vibrations were seen in the spectra from other samples but usually with lower intensity. The secondary structure assignment of band components in the spectra obtained from human TSEs was performed in analogy with the assignment of PrP27-30 from hamster TSEs. All samples from sCJD patients (except the measurement of sample Bn155a),

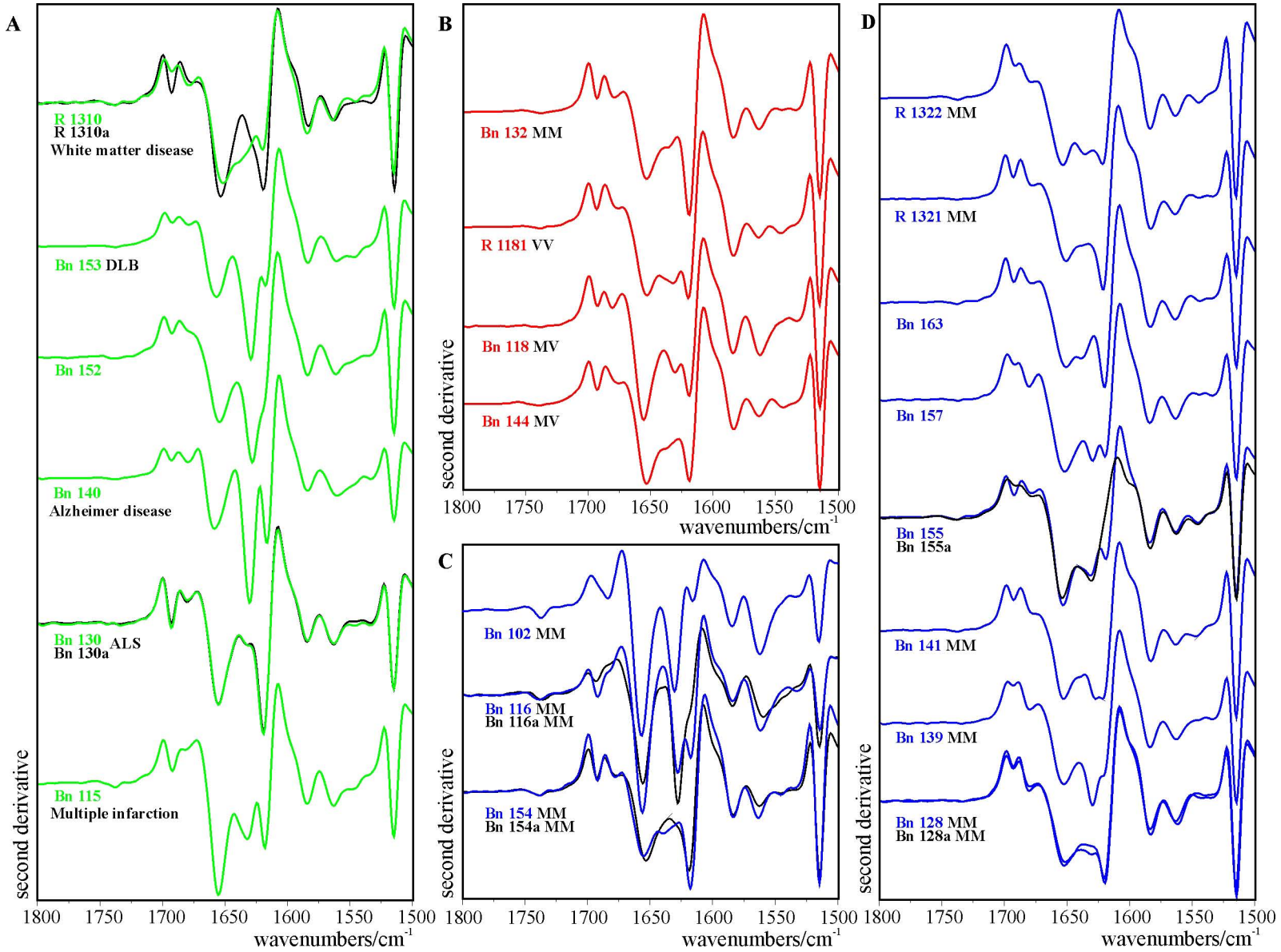

Figure 3.30 FT-IR second derivative spectra of samples purified from human brain tissue Green labels- non-CJD samples / Blue labels- type 1 PrP^{Sc} / Red labels- type 2 PrP^{Sc} / Black labels- repeatedly purified samples from identical human donors.

Table 3.V Peak position (cm^{-1}) of the most intense amide I absorption bands and second derivative characteristics of FT-IR spectra obtained from PK resistant protein fractions purified from human brain samples. Tentative assignment to protein secondary structures

Sample designation	Absorption maximum	β-sheet	Turns/β-sheet	α- Helix	β-sheet	
BN 102	1652	~1691*	1684	1657	1631	1616
BN 115	1646	1693	1682	1655	1632	1618
BN116	1653	1693	~1682*	1657	1628	1618
BN116a	1649 1632	1693	1681	1657	1628	1619*
BN118	1646	1693	1681	1656	1631	1619
BN 128	1639	1693	1680	1652	1631	1620
BN 128a	1639	1694	1681	1653	~1633*	1620
BN 130	1642	1693	1681	1655	1632	1619
BN 130a	1644	1693	1680	1655	~1632*	1619
BN 132	1641	1693	1679	1653	~1637*	1619
BN 139	1639	1694	1680	1653	1630	~1622*
BN 140	1632	1693	1680	1659	1630	1617
BN 141	1640	1693	~1678*	1653	~1640* 1628	1622
BN 144	1644	1693	1676	1653	~1637*	1619
BN 152	1636	1693	1679*	1655	1629	1620*
BN 153	1634	1693	1680	1657	1630	1618
BN 154	1640	1693	1678	1656	1640	1618
BN 154a	1642	1693	1677	1654	~1628*	1619
BN 155	1644	1693	1679	1654	1632	1619
BN 155a	1642	1691	1678	1654	1631	-
BN 157	1643	1692	1681	1652	1630	1620
BN 163	1641	1693	1679	1651	1639	1620
R 1181	1640	1693	1676	1653	1632	1620
R 1310	1643	1693	1679	1652	~1639 ~1630*	1620
R 1310a	1645	1693	1677	1654	1626*	1620
R 1321	1640	1693	1678	1651	1638*	1621
R 1322	1642	1692	1679	1654	1636	1622

*-shoulders
Green labels- non-CJD samples / Blue labels- type 1 PrP^{Sc} / Red labels- type 2 PrP^{Sc}

showed a band component between 1616 and 1622 wavenumbers, which reflects the intermolecular hydrogen bonded β-pleated structures. Characteristic intensity changes of the FT-IR second derivative contour of samples before and after treatment with PK (Figure 3.27) suggested that the high frequency β-sheet component located between 1691 and 1693 cm^{-1}

indicates an antiparallel ordering of the intermolecular β-sheet structures. The second low frequency β-sheet band was most probably associated with intramolecular hydrogen bonds. The latter was not always clearly seen as typical for prion rods from hamster TSEs. The sCJD samples were characterized by a pronounced α-helix absorption between 1651 and 1657 cm^{-1}. The second derivative spectra are characterized by a weak band component, sometimes seen as a shoulder at a position (1676- 1684 cm^{-1}) characteristic for turns and/or a high frequency β-sheet band component presumably shifted due to the H/D exchange. The protein content of samples from patients suffering from different non-CJD neurodegenerative diseases showed FT-IR absorption components characteristic for protein aggregates i.e. an intermolecular β-sheet band between 1616-1620 cm^{-1}, a component at ~1693 cm^{-1} and an overall secondary structure composition, similar to the observed in the spectra from sCJD samples (Figure 3.30 A).

3.6.1.5 Secondary structure characteristics of samples with common disease, genetic and biochemical characteristics

The spectra obtained from samples classified as PrP^{Sc} type 2 showed considerable variations in the characteristics of the band components even between patients with common codon 129 polymorphism (Bn118, Bn144) (see Figure 3.30 B, Table 3.V). The intermolecular β-sheet band of these samples was centered at 1620-1619 cm^{-1} and showed significantly different intensities. The band component indicative for intramolecular β-sheets was barely seen at 1637 cm^{-1}, as a week shoulder of the broad band typical for α-helices in the spectra of Bn132 and Bn144, and was present as a distinct component in the spectra of Bn118 and R1181 at 1631 and 1632 cm^{-1}, respectively. The specific spectral contour of sample R1181 indicated the existence of an unresolved secondary structure component/s between 1633 and 1642 wavenumbers. Although the α-helical band component in the spectra of Bn132, Bn144 and R1181 was centred at 1653 cm^{-1}, it was characterized by individual variations in the curve shape and intensity. All samples assigned to PrP^{Sc} type 2 showed variations in the turn absorption characteristics. The band component attributed to high frequency β-sheet showed common absorption frequency and band intensity. Despite that the measurements were performed in D_2O, the high frequency β-sheet component was present as intense band centred at 1693 cm^{-1} in the spectra of all four samples.

In general, all samples with glycosylation pattern typical for type 1 PrP^{Sc} were from MM homozygous individuals. However, the FT-IR second derivative spectra of these protein samples showed significant secondary structure variations (Figure 3.30 C and D). Panel C of Figure 3.30 represents the PrP27-30 spectra obtained from patients with prolonged disease duration. However, despite the common PrP genetic and clinical characteristics these samples differed significantly in their band component characteristics. The spectrum from sample Bn102 showed a small band component, centred at 1616 cm^{-1}, which could be indicative for strong intermolecular hydrogen bonded β-pleated structures and an intramolecular β-sheet band at 1631 cm^{-1}. The most intense component in the second derivative spectra from this sample was a sharp α-helical band component, centred at 1657 wavenumbers. The second derivative spectra showed the presence of turns and almost no high frequency β-sheet absorption. The main differences between the spectra obtained from samples Bn102 and Bn116 were in the relative intensity of the intermolecular β-sheet band centred at 1618 cm^{-1} in the spectrum of the last sample. In addition both spectra differed in the intensity of the high frequency β-sheet band at 1691 and 1693 cm^{-1}. Both spectra were characterised by an intense low frequency β-sheet band at 1631 and 1628 cm^{-1}, respectively.

The spectral pattern of the second derivative of sample Bn154 appear to be closer to these of samples Bn132 and Bn144 rather than to one of the other PrP^{Sc} type 1 samples. The relative intensity of the tyrosine band in the spectra of sample Bn154 was found to be significantly higher than in the samples Bn102 and Bn116, indicating a different amino acid composition of the specimen due to variations in the PK digestion site of the PrP^{Sc} molecules or in protein contents. Indeed as described above, also subtle variations in the glycosylation patterns of these samples were observed (Figure 3.28).

The remaining spectra from type 1 PrP^{Sc} shown in Figure 3.30 D also showed variations in the band component characteristics. The high frequency β-sheet component in these spectra located in the range of 1692-1694 cm^{-1}, was characterised by significant intensity variations, which in most of the spectra were obviously related to the intensity of the intermolecular β-sheet band centred in the range of 1622-1618 wavenumbers. Not clearly resolved low frequency β-sheet absorption in the range 1631-1628 cm^{-1} was observed in some of the spectra included in this group (i.e. Bn141, Bn128). In contrast to the characteristic amide II´ absorption differences observed in the PrP27-30 samples from hamster-adapted TSEs suspended in D_2O, the human samples showed only minor variations in the amide II´

absorption region as seen on Figure 3.30. Also, characteristic amide A absorption features was not found between the analyzed samples.

3.6.1.6 Spectra reproducibility

Some FT-IR spectra of samples from identical patients but obtained in independent runs (as Bn154 and Bn154a, Bn130 and Bn130a, Bn128 and Bn128a) showed fairly high spectral reproducibility (see Figure 3.31).

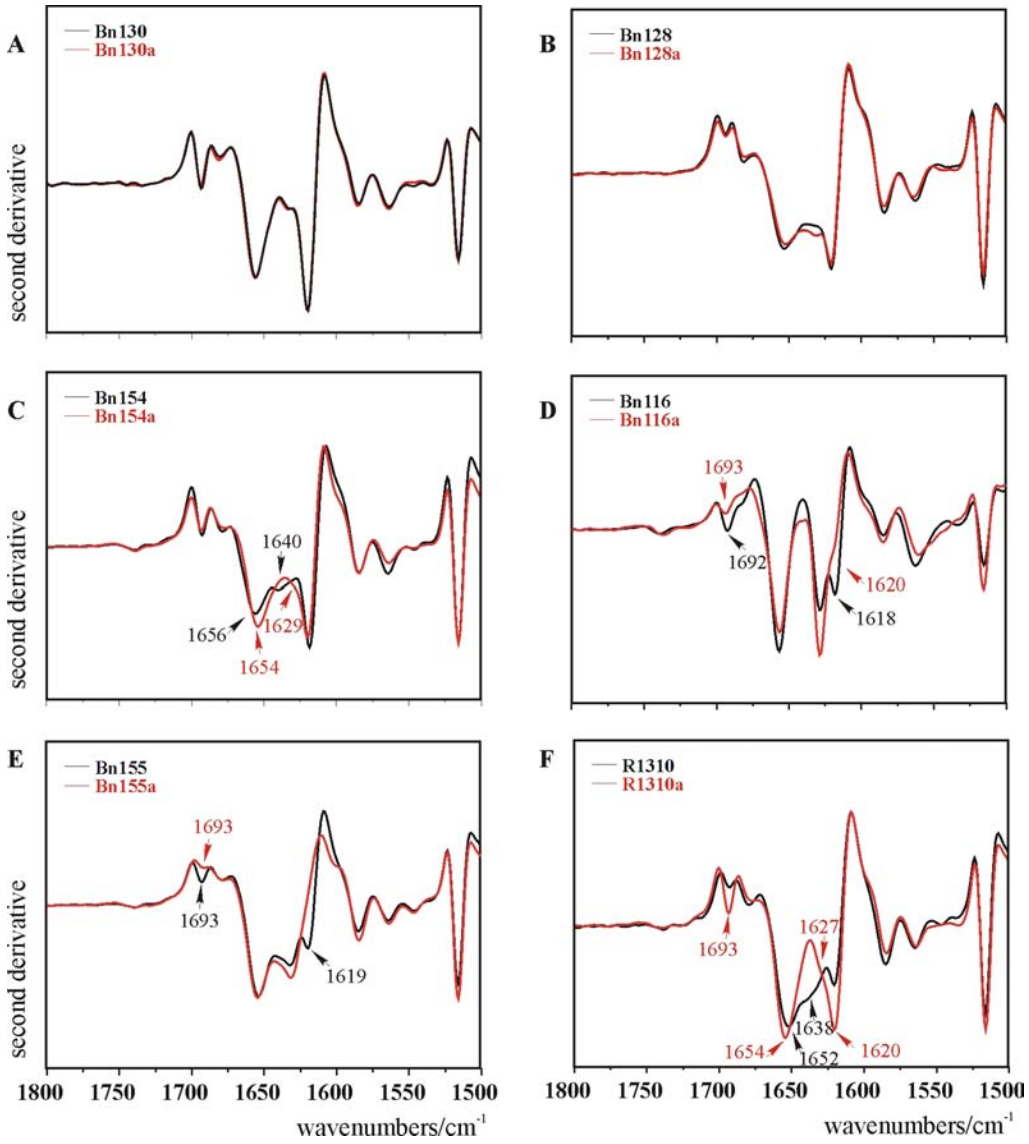

Figure 3.31 Spectra reproducibility of protein samples purified from identical human brain donors in independent purification runs

However, measurements of material from other samples (as Bn116 and Bn116a, Bn155 and Bn155a or R1310 and R1310A) showed significant variations in the second derivative features in the spectra obtained in independent purification runs, although, the

spectra from Bn116 and Bn116a samples showed certain similarities. These two differed mainly in the intensity of the β-sheet specific bands at 1619 and 1693 cm^{-1}, which were present significantly weaker intensity in the spectra from sample Bn116a. It should be reminded that the properties of the homogenized material from these two samples characteristically differed (see section 3.6.1 above). Unexpectedly, in the spectra obtained from Bn155a there were no indications for intermolecular β-sheet features (previously indicated by band components at 1619 cm^{-1} and 1693 cm^{-1} (see Figure 3.31). In contrast to sample R1310, the spectrum of sample R1310a was characterized by the presence of more distinct bands at 1620 and 1693 cm^{-1}, suggesting the presence of aggregated protein molecules in the brain from patient suffering from a white matter disease. The varying reproducibility of the second derivative FT-IR absorption characteristics suggested occasional variations in the protein composition of slightly different brain regions, and possible effects of the particular disease phenotype and/or patient individuality on the amounts and the distribution of PrP^{Sc} and protein contaminants in the brain tissue.

3.6.2 Cluster analysis

The hierarchical cluster analysis of the 27 human samples based on the normalized second derivative FT-IR spectra (Figure 3.32 A-C, next page) showed that the sCJD samples were constantly grouped in three main clusters, suggesting the presence of three main PrP27-30 secondary structure families. However, second derivative spectra obtained from CJD type 1, type 2 and non-CJD samples, are often grouped in different clusters, each time when different frequency ranges were used for the discriminative analysis (Figure 3.32 A-C). The single clusters within the different dendrograms are composed of spectra showing clearly different PrP27-30 glycosylation patterns or in some cases even merged with the spectra from non-CJD patients. These results were in striking contrast with the very reproducible and objective classification of the spectra obtained from different hamster-adapted TSEs, since the use of different spectral ranges influenced only the degree of the class internal or external heterogeneity levels between spectra obtained from independent preparations and from different strains, but did not reflect the consistency of the strain discrimination.

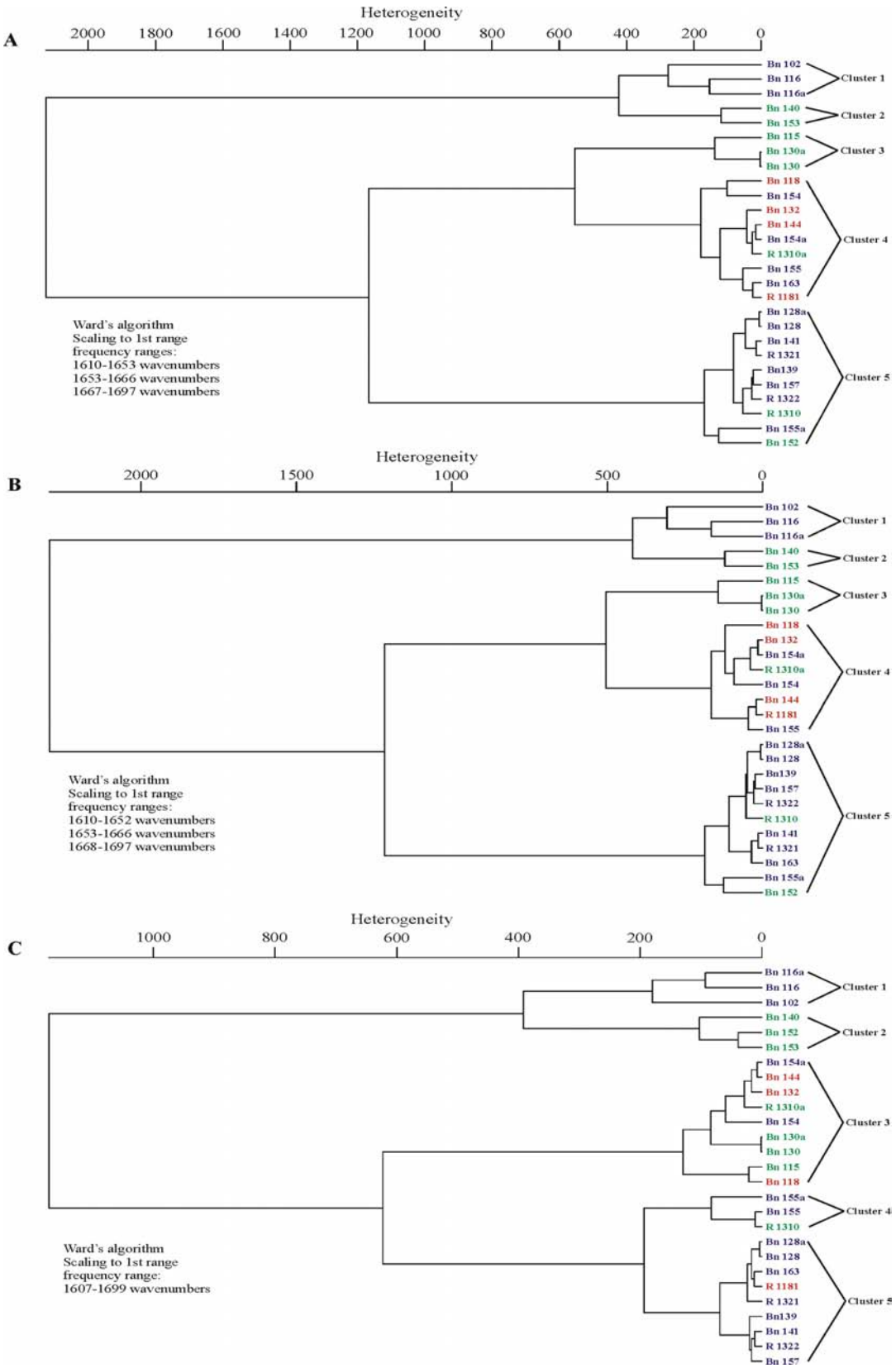

Figure 3.32 Dendrogram showing sample specific spectral diversity in the amide I region (1600-1700 wavenumbers) as observed by hierarchical cluster analysis of normalized second derivative protein spectra obtained from 27 human brain samples. Green labels- non-CJ D samples / Blue labels- type 1 PrP^{Sc} / Red labels- type 2 PrP^{Sc}. Panels A-C showed variations in the resulting clusters due to the different frequency range used to compare the spectra.

In order to evaluate the discrimination ability of the FT-IR technique, and the influence of the possible conformational heterogeneity of PrP27-30 on the spectral pattern, analysis of how a mixture of PrP27-30 from different structural types altered the second derivative FT-IR spectra was carried out. The influence of the structural heterogeneity of the PrP27-30 samples on the FT-IR spectral profile could be best investigated by mixing PrP27-30 from clearly different hamster-adapted TSE strains. Aliquots, each containing 10 µg PrP27-30 from ME7-H and 263K were diluted in 100 µl Z/D_2O. Both suspensions were combined and vortexed. The PrP27-30 mixture (200 µl) was diluted in 1 ml Z/D_2O and processed for FT-IR measurement in D_2O as described in Materials and Methods (section 2.4.2).

The second derivative FT-IR spectrum of the PrP27-30 mixture from 263K and ME7-H shows structural features slightly different from the two "pure" strains (Figure 3.33). The most significant, is the frequency shift of the intramolecular β-sheet band centered at 1636 cm^{-1}.

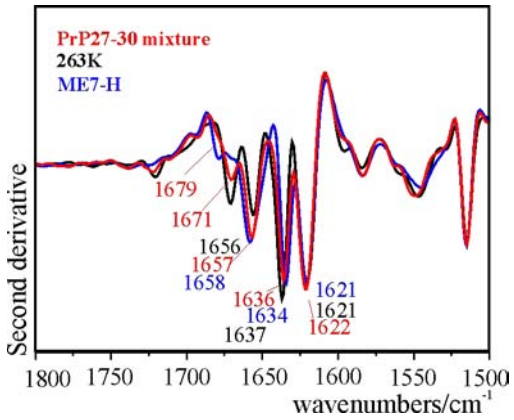

Figure 3.33 FT-IR second derivative spectra of the PrP27-30 mixture (red curve) prepared from hamster adapted TSE strains 263K (black curve) and ME7-H (blue curve). Spectra were normalized between 1600-1750 wavenumbers.

In addition the spectrum of the PrP27-30 mixture shows intermediate intensity levels of the turns and turns plus high frequency β-sheet bands at 1671 and 1679 cm^{-1} respectively. Interestingly, the spectral identity of the PrP27-30 mixture strongly depended on the frequency ranges used for the hierarchical cluster analysis (Figure 3.34).

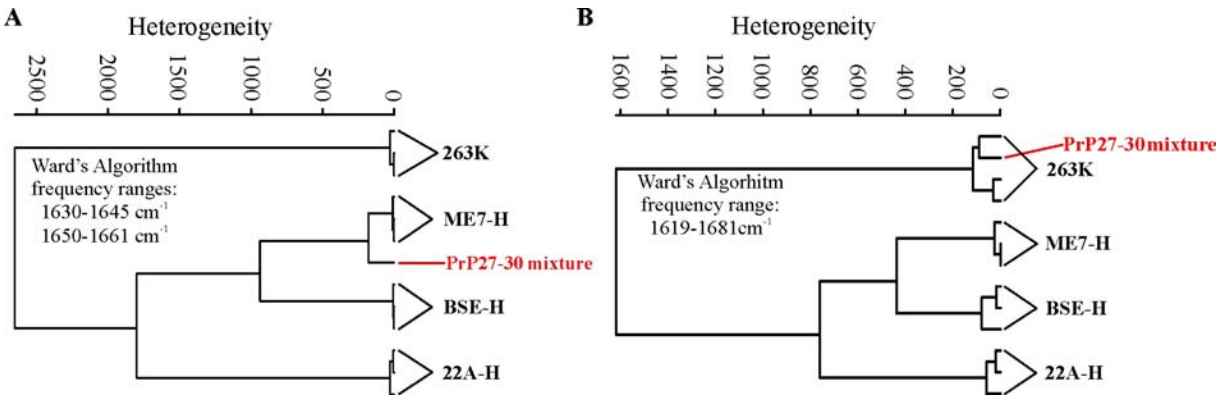

Figure 3.34 Dendrograms showing controversial classification of the PrP27-30 mixture to ME7-H (panel A) or 263K (panel B) strain, depending on the selected spectral range (ranges).

The investigation of the PrP27-30 mixture suggests that multiple conformations in a single diseased brain would be an obstacle for the objective structural discrimination of such samples. The correct strain discrimination can be additionally complicated if the proportions between the structures differ from sample to sample.